TI Designs

$PM_{2.5}$/PM_{10} Particle Sensor Analog Front-End for Air Quality Monitoring Design

TI Designs

This TI Design provides an analog front-end (AFE) solution for measuring $PM_{2.5}$ and PM_{10} particulate matter (PM). The design detects the light scattered by particles suspended in air. A sample software algorithm is provided to convert the analog output of the design into a particle size and concentration measurement. Test result data for cigarette smoke, Arizona dust, and mulberry pollen are provided along with all software and hardware design files.

Design Resources

TIDA-00378	Design Folder
INA132	Product Folder
OPA2320	Product Folder
OPA320	Product Folder
MSP-EXP430G2	Product Folder

TI E2E™ Community — ASK Our E2E Experts

Design Features

- AFE Design for $PM_{2.5}$ (<2.5-µm) and PM_{10} (<10-µm) Particle Detection and Count
  - Dust Range From 12 to 35 pcs/cm^3
  - Accuracy of 75% Over Detection Range
- AFE With Transimpedance Amplifier Stage and Two Filtering and Amplification Stages
  - 0-V Bias to Minimize Photodetector Noise and Stabilize Performance Over Temperature
  - Instrumentation Amplifier Topology to Reject External Noise Sources
  - Rail-to-Rail Output for Increased Output Dynamic Range
  - Low-Noise, Low-Input Bias Current, and Low-Offset Op Amps to Maintain High SNR
  - Adjustable Gain on Each Amplification Stage
- Tested Against Arizona Dust, Mulberry Pollen, and Cigarette Smoke Using Adapted ANSI/AHAM AC-1-2013 Test Standard
- Full Algorithm Source Code for $PM_{2.5}$ and PM_{10} Calculation
- LED Driver With Adjustable Current

Featured Applications

- Building Automation — Air Quality Monitors

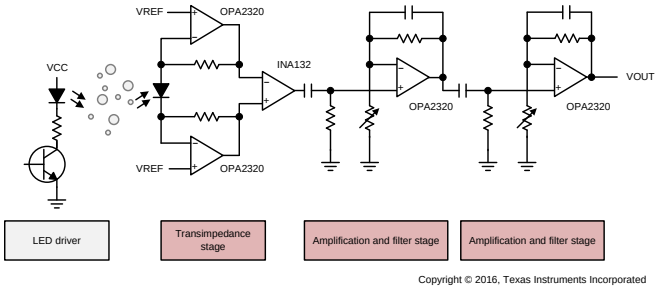

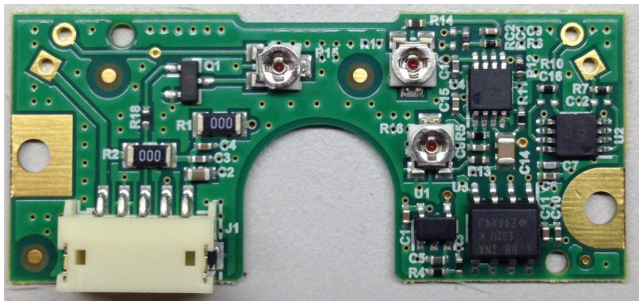

An IMPORTANT NOTICE at the end of this TI reference design addresses authorized use, intellectual property matters and other important disclaimers and information.

1 Key System Specifications

Table 1. Key System Specifications

PARAMETER	SPECIFICATION	DETAILS
Particle types and sizes detectable by the AFE	Cigarette smoke particles (0.10- to 1.0-µm diameter) Dust particles (0.5- to 3-µm diameter) Pollen particles (5- to 11-µm diameter)	Section 6
Particle concentration range supported by AFE	Pollen: 5 to 40 pcs/cm^3 Dust: 10 to 255 pcs/cm^3 Smoke: 12,000 to 24,000 pcs/cm^3	Section 6
Particle concentration measurement accuracy(1)	Dust: 75% accuracy over a PM_{10} concentration of 12 to 35 pcs/cm^3 (using linear calibration and a 60-second moving average)	Section 6
AFE input voltage	3.3 V, nominal	Section 4.3
AFE current consumption	13 mA, average	Section 6.9
LED driver current consumption	Adjustable	Section 4.4
Form factor	44 × 19 mm	Section 7.5

(1) Accuracy calculated using high-resolution, real-time aerodynamic TSI 3321 Aerodynamic Particle Sizer Spectrometer as reference.

2 System Description

Different methods exist to measure the amount of particle matter (PM) suspended in air. Optical-based PM measurement instruments utilize the properties of absorption and light scattering to measure particle count, size, and concentration. Although these instruments differ in complexity, accuracy, and cost, they all share the same basic components: a light source directed at the particles, a detector to measure the light scattered (or absorbed) by the particles, an AFE to interface with the detector, and signal processing to analyze the output of the AFE.

The $PM_{2.5}$/PM_{10} Particle Sensor Analog Front-End Design is capable of detecting particle matter with a diameter between 2.5 and 10 µm (PM_{10}) and particle matter with a diameter less than 2.5 µm ($PM_{2.5}$). This TI Design filters and amplifies the output from a photodiode and produces an output signal that can be processed by a microcontroller. The transimpedance stage uses an OPA2320 dual-package precision CMOS operational amplifier (op amp) and an INA132 single-supply difference amplifier to convert the output current of the photodetector into a voltage. The filter and amplification stages use the OPA2320 op amp with a tunable gain and basic RC-filters. A light-emitting diode (LED) driver with an adjustable LED current is also included in the design.

The design is implemented on a single-ended, four-layer board of a size of 44 × 19 mm with a build-of-materials (BOM) count of 37 components. The TI Design interfaces with the photodiode and LED of an existing optical chamber through dedicated pads on the board. This TI Design was tested using pollen, dust, and smoke particles—the full test procedure and results are included in this design guide.

This design guide addresses component selection, design theory, and test results of the entire TI Design system. The information provided in this design guide gives system designers a fully-tested reference design, which can be easily modified to meet different system requirements.

3 Block Diagram

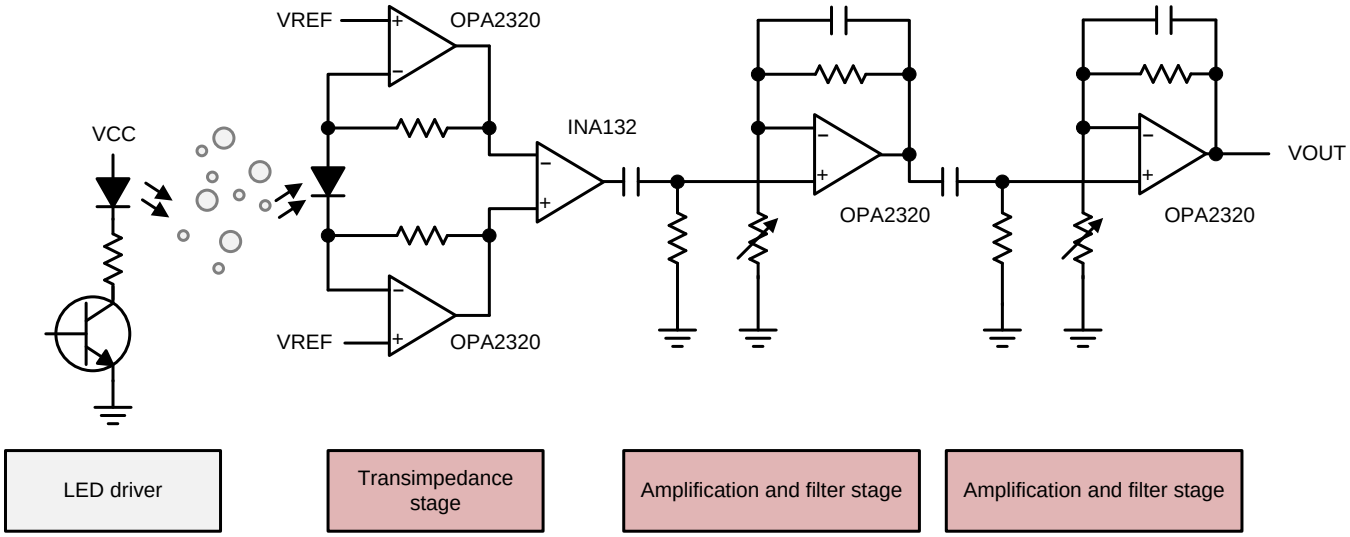

Figure 1. Particle Sensor Block Diagram

3.1 Highlighted Products

The $PM_{2.5}$/PM_{10} Particle Sensor AFE Design features the following devices:

- OPA2320 and OPA320 (Section 3.1.1): precision, 20-MHz, 0.9-pA bias current, rail-to-rail I/O, CMOS op amp
- INA132 (Section 3.1.2): Low-power, single-supply difference amplifier

For more information on each of these devices, see their respective product folders at www.ti.com.

3.1.1 OPA320 and OPA2320 Description

The OPA320 (single) and OPA2320 (dual) are a new generation of precision, low-voltage CMOS op amps optimized for very low noise and wide bandwidth while operating on a low quiescent current of only 1.45 mA.

The OPA320 series is ideal for low-power, single-supply applications. Low-noise (7 nV/√Hz) and high-speed operation also make them well-suited for driving sampling analog-to-digital converters (ADCs). Other applications include signal conditioning and sensor amplification.

The OPA320 features a linear input stage with zero-crossover distortion that delivers excellent common-mode rejection ratio (CMRR) of typically 114 dB over the full input range. The input common-mode range extends 100 mV beyond the negative and positive supply rails. The output voltage typically swings within 10 mV of the rails.

In addition, the OPA320 and OPA2320 have a wide supply voltage range from 1.8 to 5.5 V with excellent PSRR (106 dB) over the entire supply range, making them suitable for precision, low-power applications that run directly from batteries without regulation.

The OPA320 (single version) is available in a SOT23-5 package; the OPA320S shutdown single version is available in an SOT23-6 package. The dual OPA2320 is offered in SO-8, MSOP-8, and DFN-8 packages, and the OPA2320S (dual with shutdown) in an MSOP-10 package.

3.1.1.1 OPA2320 and OPA320 Features

- Precision with zero-crossover distortion:
  - Low offset voltage: 150 µV (max)
  - High CMRR: 114 dB
  - Rail-to-rail I/O
- Low-input bias current: 0.9 pA (max)
- Low noise: 7 nV/√Hz at 10 kHz
- Wide bandwidth: 20 MHz
- Slew rate: 10 V/µs
- Quiescent current: 1.45 mA/ch
- Single-supply voltage range: 1.8 to 5.5 V
- OPA320S, OPA2320S: I_Q in shutdown mode: 0.1 µA
- Unity-gain stable
- Small packages: SOT23, MSOP, DFN

3.1.2 INA132 Description

The INA132 is a low-power, unity-gain differential amplifier consisting of a precision op amp with a precision resistor network. The on-chip resistors are laser trimmed for accurate gain and high common-mode rejection. Excellent TCR tracking of the resistors maintains gain accuracy and common-mode rejection over temperature. The internal op amp's common-mode range extends to the negative supply—ideal for single-supply applications. It operates on single (2.7 to 36 V) or dual supplies (±1.35 to ±18 V).

The differential amplifier is the foundation of many commonly used circuits. The INA132 provides this circuit function without using an expensive precision resistor network. The INA132 is available in 8-pin DIP and SO-8 surface-mount packages and is specified for operation over the extended industrial temperature range, –40°C to 85°C.

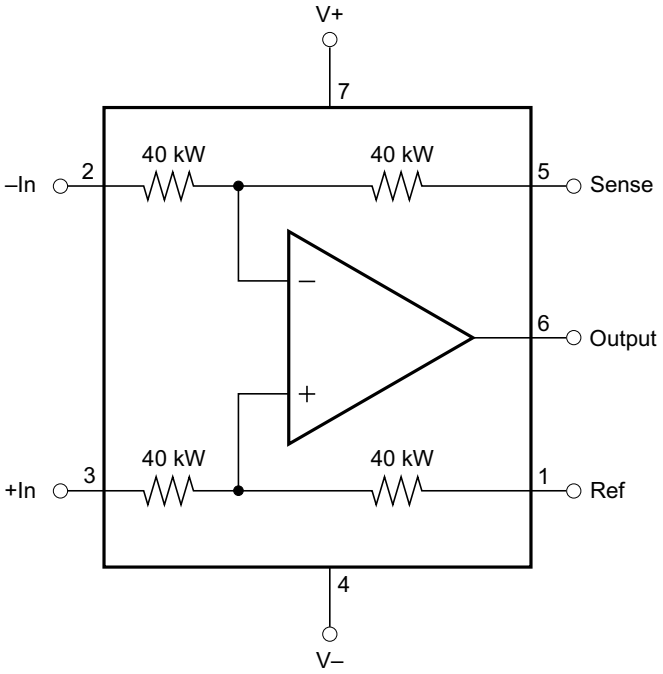

Figure 2. INA132 Block Diagram

3.1.2.1 INA132 Features

- Low quiescent current: 160 µA
- Wide supply range:
  - Single supply: 2.7 to 36 V
  - Dual supplies: ±1.35 to ±18 V
- Low gain error: ±0.075% max
- Low nonlinearity: 0.001% max
- High CMR: 90 dB
- Highly versatile circuit
- Easy to use
- Low cost
- 8-pin DIP and SO-8 packages

4 System Design Theory

This section briefly discusses important aspects of PM and optical-based measurement approaches. A detailed description of the design theory behind the $PM_{2.5}$/PM_{10} Particle Sensor AFE Design is also included in this section.

4.1 Background on Particulate Matter

The term "particulate matter" or "particle pollution" refers to a mixture of very small particles found in the air. These small particles can be inhaled, where they affect the heart and lungs and can cause serious health effects. Particles with a diameter of 10 µm or less are of most concern because they can pass through the nose and throat and enter the lungs.

In the United States, the Environmental Protection Agency (EPA) groups PM into two categories based on the size of the particle diameter. Particles with a diameter between 2.5 and 10 µm are labeled as "inhalable coarse particles". Particles with a diameter less than 2.5 µm are labeled as "fine particles". Coarse particles pose a health risk because they can accumulate in the respiratory system. Sources for coarse particles include grinding or crushing operations, dust stirred up by driving cars, pollen, and mold. Fine particles pose an even greater health risk than coarse particles because they can travel deeper into the lungs due to their small size. These particles are generated from combustion sources such as forest fires, power plants, and automobiles as well as organic compounds and metals.

The EPA sets standards for acceptable concentrations of $PM_{2.5}$ and PM_{10} particulate matter in the United States through the National Ambient Air Quality Standard (NAAQS) for Particulate Matter. The term $PM_{2.5}$ refers to all particles that are 2.5 µm in diameter and smaller, while PM_{10} refers to all particles smaller than 10 µm. As of 2012, the NAAQS sets the annual $PM_{2.5}$ standard at 12 µg/m^3 and the 24-hour $PM_{2.5}$ standard at a level of 35 µg/m^3. The 24-hour PM_{10} is set at 150 µg/m^3. Table 2 shows PM standards in other parts of the world.

Table 2. PM Permissible Levels Around The World

ORGANIZATION	$PM_{2.5}$ PERMISSIBLE LEVELS		PM_{10} PERMISSIBLE LEVELS	
	ANNUAL MEAN	24-HOUR MEAN	ANNUAL MEAN	24-HOUR MEAN
World Health Organization	10 µg/m^3	25 µg/m^3	20 µg/m^3	50 µg/m^3
European Union	25 µg/m^3	—	40 µg/m^3	50 µg/m^3
USA (EPA)	12 µg/m^3	35 µg/m^3	—(1)	150 µg/m^3

(1) Note that there is no annual PM_{10} standard—a previous annual PM_{10} standard was revoked by the EPA in 2006 due to lack of evidence linking long-term exposure to coarse particles and health problems.

The NAAQS also describes the conversion between the air quality index (AQI) for a given PM concentration. The AQI is reported daily to inform residents of the level of pollution in the air. Multiple pollutants, including PM concentration, are used to determine the AQI. To calculate the AQI, each pollutant is translated into a corresponding AQI value and the highest value is used as the final AQI number. An AQI below 100 is considered satisfactory, whereas values above 100 are considered unhealthy. Table 3 gives the corresponding AQI values for concentrations of $PM_{2.5}$ and PM_{10} concentrations as provided by the EPA.

Table 3. Corresponding AQI Categories For Different PM Concentrations(1)

$PM_{2.5}$ (µg/m^3) 24-HOUR	PM_{10} (µg/m^3) 24-HOUR	AQI	CATEGORY
0.0 to 12.0	0 to 54	0 to 50	Good
12.1 to 35.4	55 to 154	51 to 100	Moderate
35.5 to 55.4	155 to 254	101 to 150	Unhealthy for sensitive groups
55.5 to 150.4	255 to 354	151 to 200	Unhealthy
150.5 to 250.4	355 to 424	201 to 300	Very unhealthy
250.5 to 350.4	425 to 504	301 to 400	Hazardous
350.5 to 500.4	505 to 604	401 to 500	Hazardous

(1) Only AQI categories for $PM_{2.5}$ and PM_{10} pollutants are shown in this table. For other pollutants used in the AQI calculation, see the EPA's NAAQS for PM.

4.2 Measuring PM Using Optical Techniques

There are multiple methods available for measuring PM. Some of these methods are based on inertial, gravitational, centrifugal, thermal, and optical techniques.

Optical-based PM measurement instruments utilize the properties of absorption and light scattering to measure particle count, size, and concentration. The light scattered by the particle depends on the light source, the detection angle, the particle size, the particle shape, and reflective index of the particle. These last two factors are particularly difficult to predict. Therefore, this type of PM measurement instruments can only offer approximate size information.

Photometers and optical particle counters (OPCs) are two examples of optical-based PM measurement instruments. A photometer measures the mass concentration of particles by measuring the amount of scattered light from a cloud of particles. An OPC measures the light scattered by single particles to measure their size and count.

Both types of PM measurement instruments have advantages and disadvantages. For example, although a photometer can be used with high particle concentrations, they cannot give any information about the particle size and significantly underestimate the mass contributed by large particles. On the other hand, OPCs provide size information but can have difficulty with high particle concentrations.

When coupled with an optical chamber design, the $PM_{2.5}$/PM_{10} Particle Sensor AFE Design measures the particle size and concentration in PM. The optical chamber consists of a LED pointed at a sensing area and a photodiode placed at an angle to the LED. As the particles pass through the sensing area, light from the LED is scattered by the particles and sensed by the photodiode. The output current of the photodiode is filtered and passed through two amplification stages in the design. The resulting waveform consists of several pulses of varying amplitude. The amplitude of the pulses gives an indication of the particle size, while the number of pulses is related to the particle concentration. The processing of the pulse information can be done using a microcontroller.

4.3 AFE Design

4.3.1 Transimpedance Stage

There are many circuit topologies available to implement a transimpedance amplifier stage. The choice ultimately depends on the photodiode performance optimization required by the overall system. Because this design uses the photodiode to detect the scattering of light off of particles flowing through an optical chamber, high bandwidth is not required; this allows the use of a transimpedance stage, which biases the photodiode at 0 V. The 0-V bias is important as this not only minimizes noise output from the photodiode, but also because there is no reverse bias, the leakage current of the photodiode is also avoided, which leads to stability in sensing the amount of scattered light over temperature since leakage current increases exponentially with increasing temperature. Another key aspect for this application is high sensitivity so that a wide range of particle sizes can be detected, which translates to a high signal-to-noise ratio (SNR). All of these considerations led to the transimpedance stage design shown in Figure 3.

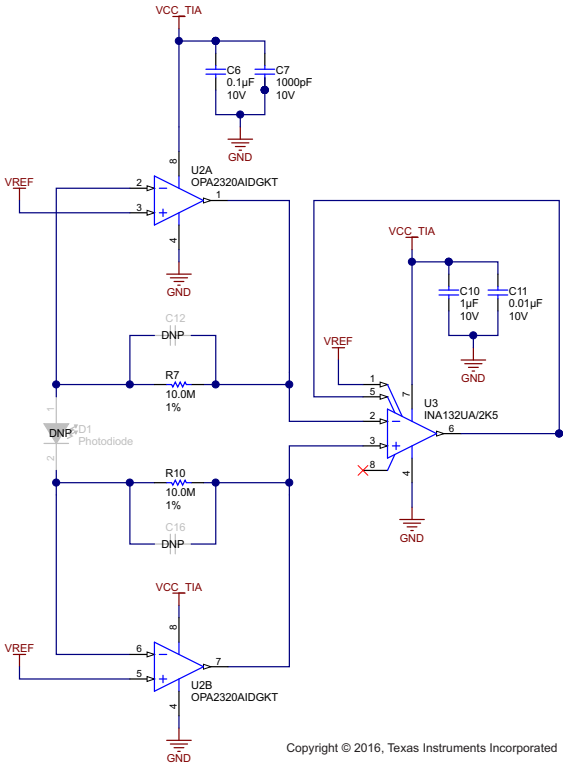

Figure 3. AFE Transimpedance Stage

As can be seen in Figure 3, this transimpedance stage achieves a 0-V photodiode bias through the virtual ground of operational amplifiers U2A and U2B. To maximize SNR, the majority of the signal gain of the overall signal path should come from the transimpedance stage because the signal gain for this stage is proportional to the value of the feedback resistor value. Compared to the thermal noise of the feedback resistors, which varies as √R, the overall SNR is then also proportional to √R. The difference amplifier (U3) converts the differential signal into a ground referenced single-ended signal prior to the filtering and voltage scaling stages.

An added benefit of this transimpedance stage is that it is inherently robust to external noise sources as long as the layout is symmetric, due to its instrumentation amplifier type topology. Because external noise will appear as common mode perturbations, these will be rejected by the difference amplifier. Even with this noise rejection technique in place, it is still necessary to shield the circuit to prevent noise due to electrostatic coupling due to the high value resistors needed for this stage.

As shown in the schematic of Figure 3, the gain at the output of this stage is, $G = V_{OUT}/i_P = R7 + R10 = 20 \times 10^6$ (V/A), where V_{OUT} is the output of U3 and i_P is the photodiode current. Capacitors C12 and C16 are included for added stability by eliminating noise gain peaking. However, these two capacitors were not populated in this design because the circuit was stable without them.

Even though this design focuses on positive peaks of current when light is scattered and the op amps being used are rail-to-rail at the input and output, it was necessary to bias this stage to mid rail because the difference amplifier is not a rail-to-rail device. This was accomplished using an additional OPA320 (not shown) in a unity gain configuration that buffers the center point of a $V_{CC}/2$ voltage divider to drive the V_{REF} signal shown. This provides a low-impedance bias voltage to the reference pin of the difference amplifier.

For additional information on transimpedance amplifiers for photodiode monitoring, see the application report *Photodiode Monitoring with Op-Amps* (SBOA035).

4.3.2 Filter and Gain Stages

Additional voltage scaling of the analog output signal is required to achieve the desired overall sensitivity. Filtering of the analog signal is necessary to limit the noise bandwidth and reduce the peak-to-peak noise at the output of the analog signal chain. The circuit shown in Figure 4 is designed to accomplish these two requirements as the final two stages of the AFE. The input to the amplified filter circuit is the output of the transimpedance stage while its output goes to the input of the ADC in the MCU to facilitate the signal processing algorithm.

The amplifiers used in this stage must have rail-to-rail operation, low offset, low noise, and low input bias current. Rail-to-rail operation allows the amplified filter stages to be ground referenced since only positive polarity changes in photodiode current are being processed. The rail-to-rail operation also allows the dynamic range to be maximized at the output of the AFE.

While these two amplified filter stages are AC coupled, it is desirable to build both stages using the same op amp. Also, because the output stage can be adjusted to have a relatively gain, this op amp should have low offset so that the output of the AFE is close as possible to the ground reference for zero photodiode current. In a similar fashion, low noise is needed to maintain the highest possible SNR by adding a minimum amount of noise to the signal chain so that the smallest possible particle size may be detectable by the system. Because of the adjustable gain and resulting large difference in resistor sizes on the op amp inputs, low input bias current is needed to prevent an additional source of offset from appearing at the output of the AFE.

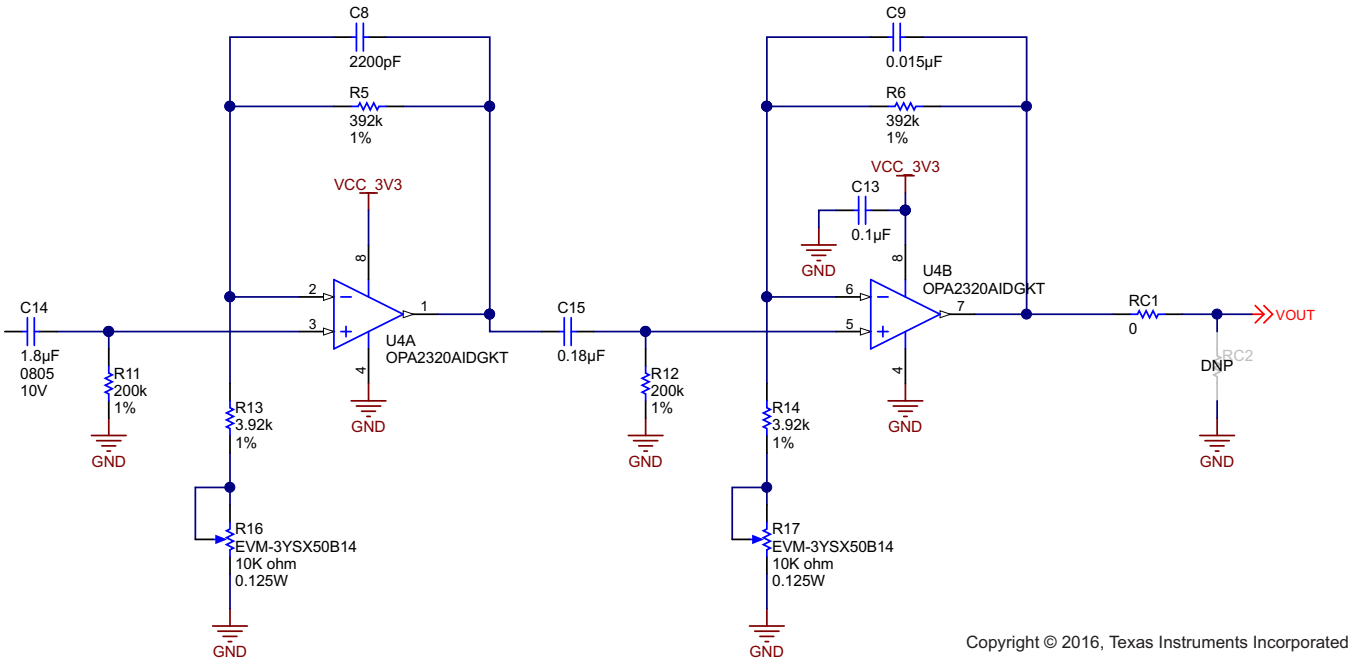

Figure 4. AFE Filter and Gain Stages

The filter response for this circuit forms a bandpass filter composed of simple poles and zeroes. The first stage is a second-order wider bandwidth bandpass filter while the second stage is a narrower bandwidth second-order bandpass filter whose cutoff frequencies lie within the pass band of the first stage. Due to this design of the filter response, the second stage determines the cutoff frequencies for the overall cascade filter while the first stage provides additional attenuation at frequencies further into the filter stop band. Because this design is measuring the scattering of light due to particles in motion through the optical chamber, the frequencies of interest and therefore the pass band of this filter can be quite low. The exact placement of the passband should be chosen to match the particle flow rate expected, especially if air is being forced through the optical chamber by means of a fan, heater element, or other means.

Additionally, the filter construction using simple poles and zeroes leads to a low Q response, which means that a narrow passband implementation results in lower passband gain than defined by the resistor ratio in each stage due to the overlapping response of the low Q poles and zeroes. Generally, the low-frequency cutoff sets the lower limit for the flow rate of particles through the optical chamber while the high frequency cutoff sets the upper limit for the particle flow rate. The placement of the high frequency cutoff also serves to limit the noise bandwidth and therefore can help in the reduction of peak-to-peak noise observed at the output of this circuit. This is especially useful where moderate to high gain is needed for voltage scaling from this part of the circuit.

In this design, the following equations can be used to make adjustments to the filter response:

Stage 1:

$$f_{low} = \frac{1}{2\pi \times R11 \times C14} = 0.44\ Hz \qquad f_{high} = \frac{1}{2\pi \times R5 \times C8} = 184.5\ Hz \tag{1}$$

Stage 2:

$$f_{low} = \frac{1}{2\pi \times R12 \times C15} = 4.4\ Hz \qquad f_{high} = \frac{1}{2\pi \times R6 \times C9} = 27\ Hz \tag{2}$$

The gain for this circuit is described as:

$$G_1 = 1 + \frac{R5}{(R13 + R16)} \qquad G_2 = 1 + \frac{R6}{(R14 + R17)} \tag{3}$$

$$G_{tot} = \left(1 + \frac{R5}{(R13 + R16)}\right)\left(1 + \frac{R6}{(R14 + R17)}\right) \tag{4}$$

By observation of Equation 4 along with Figure 4, it can be seen that the adjustable gain range for each stage is from 29 to 101.

The simulated filter response of this circuit at the maximum gain setting is shown in Figure 5. The minimum gain at high frequency is unity up to the frequency at which the amplifier response starts to roll off. For applications where this is not desirable, components RC1 and RC2 shown in Figure 4 are included so that an additional passive low-pass (or high-pass) filter could be implemented.

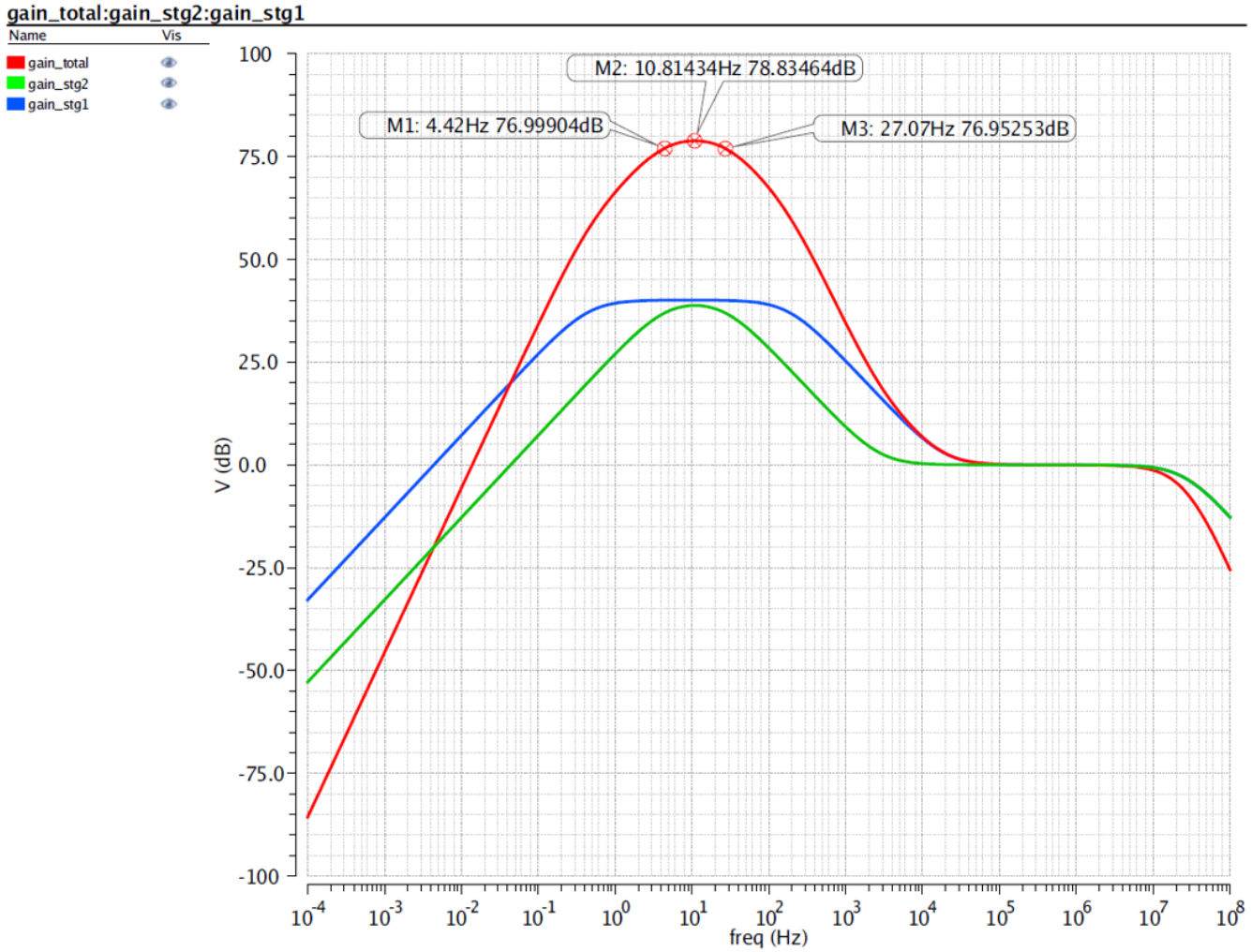

Figure 5. Simulated AFE Filter Response

This is only one of the many possible ways available to implement this filter function while achieving the same overall result. More study on the exact nature of the input signal to the system would be needed to help optimize the filter response for a given optical chamber in order to arrive at a fully optimized filter design. One tool that is available for further study of the filter implementation in this application and others is the Texas Instruments WEBENCH® Filter Designer tool.

4.4 LED Driver

As shown in Figure 6, the $PM_{2.5}$/PM_{10} Particle Sensor AFE Design uses a simple NPN transistor to create an LED driver. The collector current depends on the voltage-current characteristics of the LED (see LED datasheet). The potentiometer, R15, can adjust this forward voltage of the LED and therefore the total collector current. Additionally, the LED current can be turned on and off through the IR_LED_CTRL signal (see Table 4).

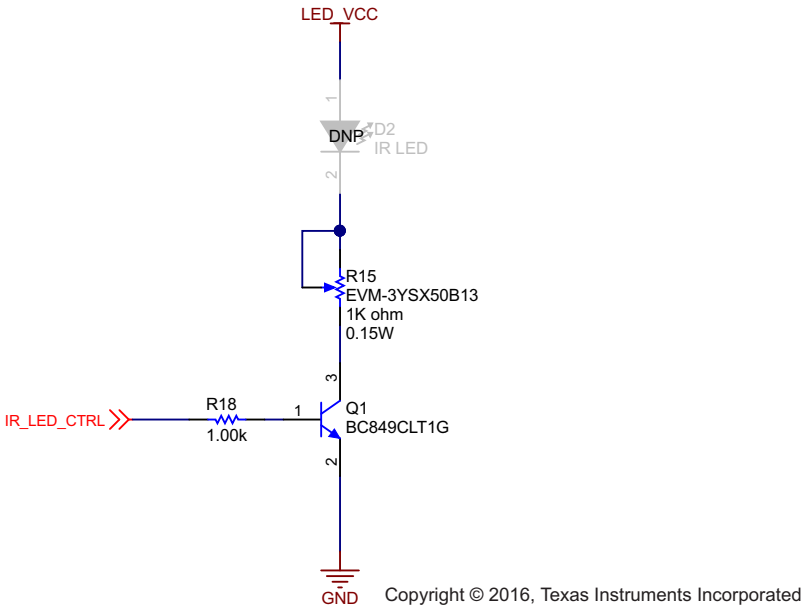

Figure 6. LED Driver

Table 4. IR_LED_CTRL Signal

IR_LED_CTRL	LED CURRENT
High	On
Low	Off

4.5 Software Algorithm

A simple software algorithm was developed to demonstrate how to use the output of the sensor to determine particle concentration and, to some extent, particle size. This section describes the theory behind the algorithm and its implementation.

4.5.1 Relationship of Pulse Height and Spacing to Particle Size and Concentration

As particles pass through the sensor, light from the LED is scattered by the particles and sensed by the photodiode. The output of the $PM_{2.5}/PM_{10}$ Particle Sensor AFE Design consists of a series of pulses that are directly related to the light scattered by the particles.

To analyze the relationship of these pulses to particle size and concentration, this TI Design (coupled with an optical chamber, see Section 6.1) was exposed to varying concentrations of these particles. The output of the design was logged for post-test data analysis. Figure 7, Figure 8, and Figure 9 show histograms of the pulse amplitude for smoke, dust, and pollen particles, respectively, over the duration of each test. A 10-bit ADC digitized the output of the $PM_{2.5}/PM_{10}$ Particle Sensor AFE Design. Each histogram divides the ADC range (20 to 1024) into bins and counts the number of pulses which fall into each bin. Note that the range 0 to 19 was deliberately left off the histogram plots because this is the noise range of the sensor (see Section 6.3 for more information on noise measurements).

An analysis of the histogram plots shows that the pulse height (amplitude) has a direct relationship to the size of the particle (that is, the sensor outputs larger pulses for larger particles). This result is expected by considering that larger particles will scatter more light compared to smaller particles. The relative sizes of the three particles are shown in Table 5.

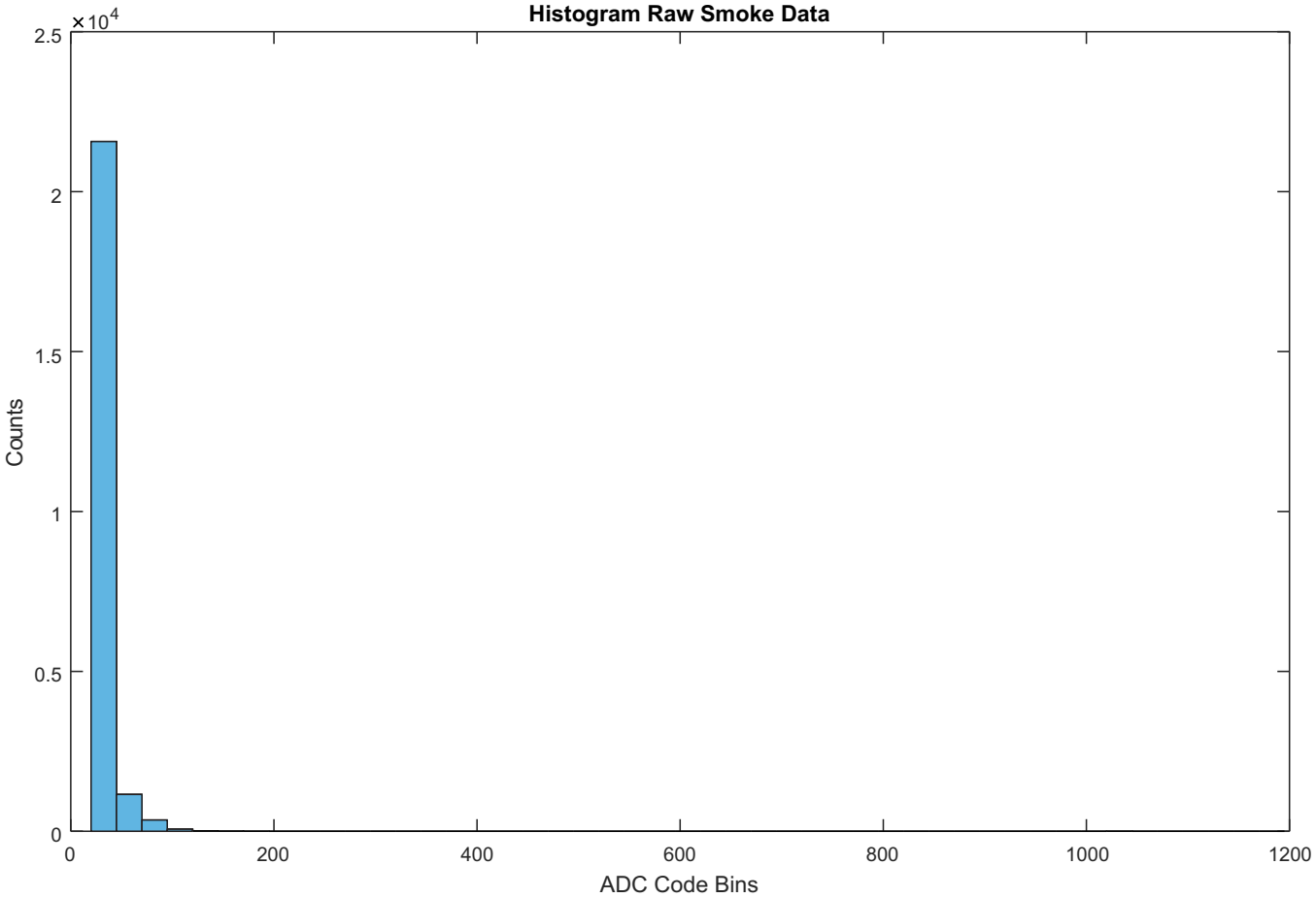

Figure 7. Histogram of ADC Codes for Smoke Particles

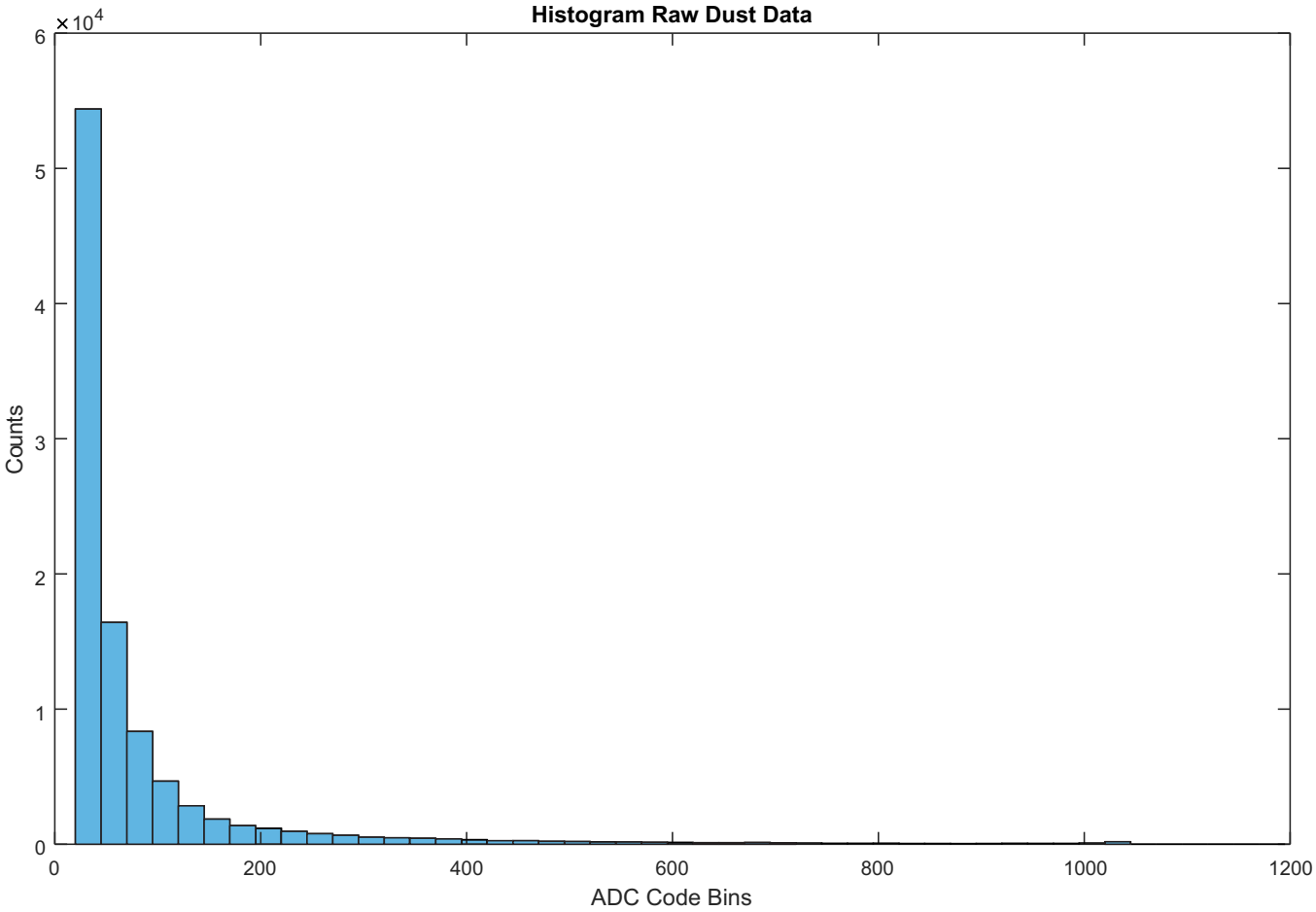

Figure 8. Histogram of ADC Codes for Dust Particles

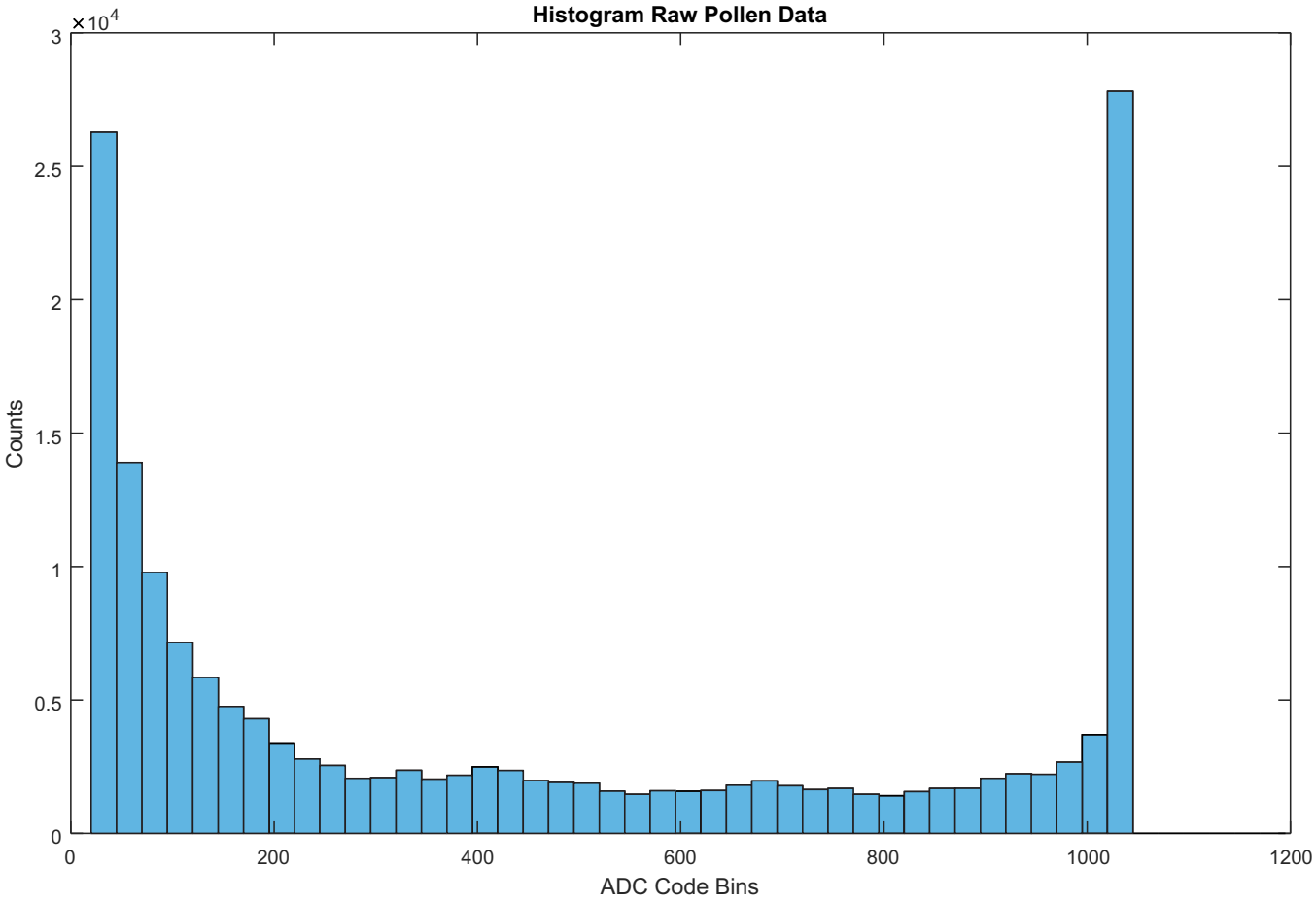

Figure 9. Histogram of ADC Codes for Pollen Particles

Table 5. Particle Sizes and Concentration

PARTICLE TYPE	SIZE (µm)	CONCENTRATION RANGES (particles/cc)	CONCENTRATION (particles/ft^3)
Pollen	5 to 11	5 to 40	~141,600 to 1,133,000
Dust	0.5 to 3	10 to 255	~283 × 10^3 to 7.233 × 10^6
Smoke	0.10 to 1.0	12,000 to 24,000	~340 × 10^6 to 680 × 10^6

On the other hand, inspecting the histogram plots shows that the particle concentration does not have a proportional impact on the pulse height. For example, the height of the pulses for dust particles were, on average, smaller than the pulses for pollen particles even though there were almost 100 times more dust particles per cubic centimeter compared to pollen particles. This observation reinforces the complex relationship that exists between particle size, particle shape, and reflective index of the particle.

The data analysis shows that particle concentration does have a direct relationship to the spacing between pulses. In other words, a higher concentration of particles generates pulses that are spaced closer together. Figure 10 plots the number of pulses above the P1 threshold in one-second intervals and the PM_{10} particle concentration at the same instant in time. Figure 10 reveals that as the particle concentration goes down, the spacing between the pulses increases and the pulse count decreases within each one-second interval.

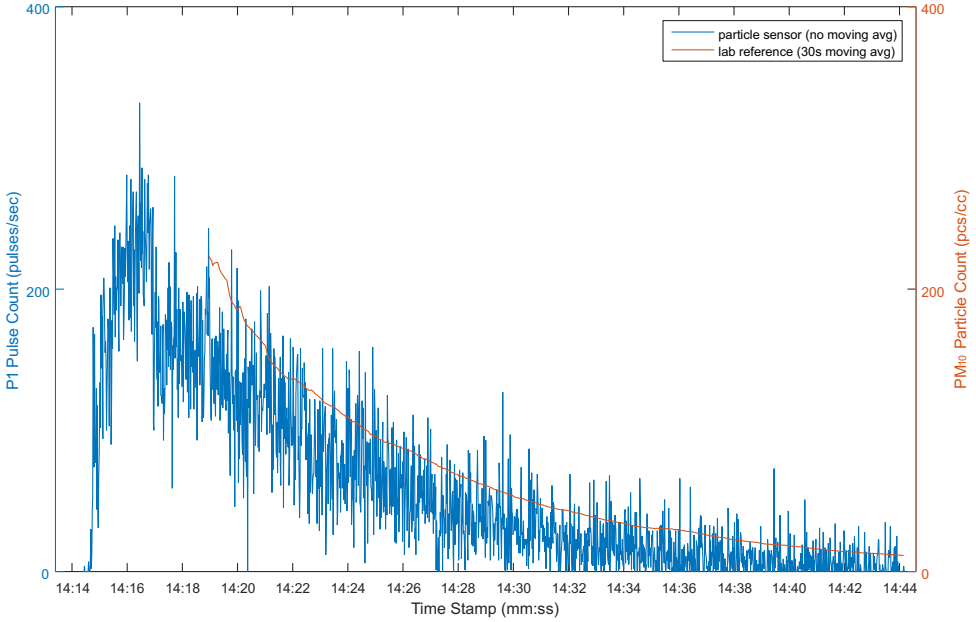

Figure 10. Pulse Count versus Particle Concentration (Dust Particles)

The relationship between pulse height and particle size, and pulse spacing and particle concentration is summarized in Figure 11.

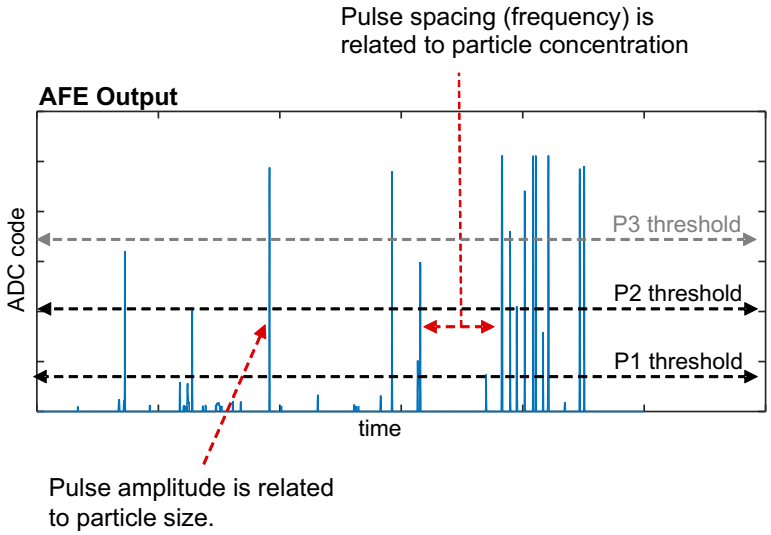

Figure 11. Pulse Spacing and Height

4.5.2 Algorithm Implementation

The software algorithm estimates the concentration of particles flowing through the sensor by measuring the pulse height and spacing of pulses generated by the $PM_{2.5}$/PM_{10} Particle Sensor AFE Design. An overview of the software algorithm is given in Figure 12.

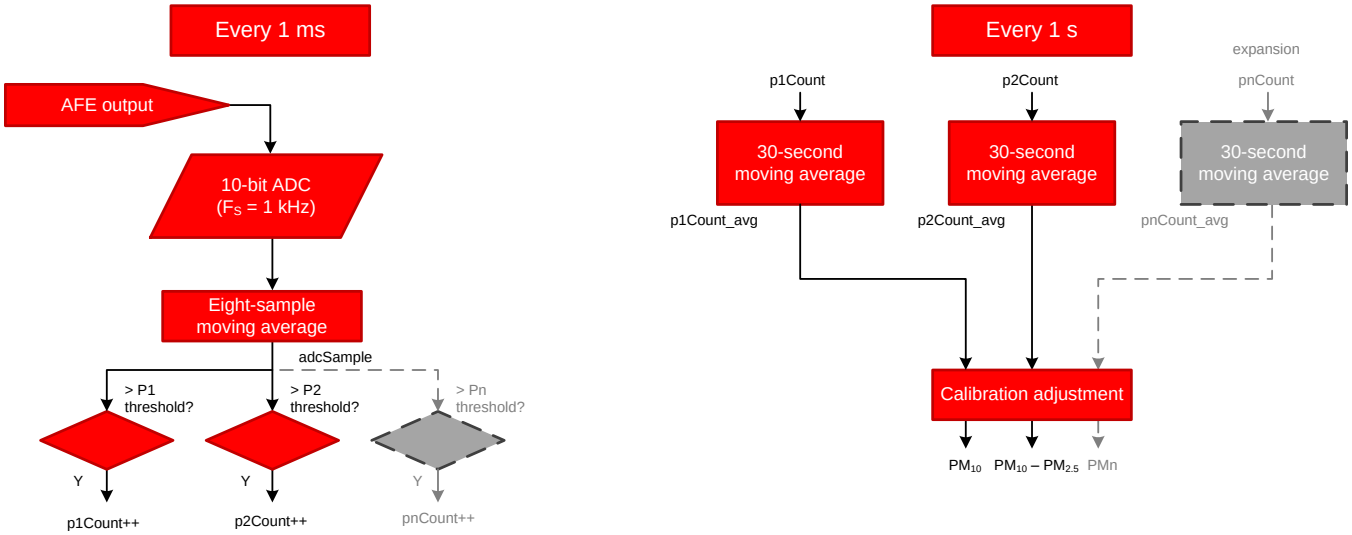

Figure 12. Sample Software Algorithm for Particle Concentration Estimation

The software algorithm samples the AFE output every 1 ms and uses an eight-sample moving average to remove some of the noise from the signal. Running counters measure the pulse count given two separate thresholds, P1 and P2. The P1 threshold filters out the sensor noise and the P2 threshold distinguishes between different sizes of particles.

Every second, the counts are passed through ten-second moving average and the resulting value is passed through a calibration linear formula. The linear formula is developed beforehand by comparing the sensor output to data taken by high-accuracy lab equipment (see Table 8) during the sensor tests.

As shown in Figure 12, the software algorithm can be expanded to detect different particle sizes through the use of multiple thresholds. This assumes the particles being tested have a predicable light scattering effect, which may not always be the case.

4.5.3 Establishing P1 and P2 Thresholds

Two thresholds are established to detect different particles sizes. The P1 threshold filters out the sensor noise and the P2 threshold distinguishes between two particle sizes. Selecting the P1 threshold is based on a simple analysis of the noise level in the sensor. On the other hand, the P2 threshold requires careful analysis of the sensor output data. In theory, it is possible to establish multiple thresholds so that multiple particle sizes can be detected. However, in practice, this method greatly depends on the light scattering effect of each particle, which may not always be easily predictable.

For the development of this software algorithm, the P2 threshold was established through analyzing the AFE output data when the sensor was exposed to varying concentrations of dust, pollen, and smoke particles. Advanced knowledge of size distribution of each particle either through literature or through measurement is a key factor in establishing each threshold.

The histogram plots given in Figure 7, Figure 8, and Figure 9 can be used to establish the P2 threshold. As seen in Figure 8, for dust particles the majority of the codes are below the value of 400. Given that dust particles vary in size between 0.5 and 3 µm, with the majority of the particles below 2.5 µm, a P2 threshold of 400 can be selected to capture the majority of pulses generated by dust particles above a size of 2.5 µm. In other words, any pulse above 400 can be assumed to be a particle larger than 2.5 µm. Similarly for smoke, the majority of the particles are below 2.5 µm and the same P2 threshold of 400 can be used. For pollen, the histogram is more complicated. This could be attributed to the fact that pollen particle are more irregular in shape and size. Therefore, in this case, it is not as straight forward to select a P2 threshold. For the purposes of this software algorithm, the P2 threshold was left at 400.

4.5.4 Relationship of P1 and P2 Thresholds to $PM_{2.5}$ and PM_{10} Particle Counts

The term PM_{10} includes all particles with a diameter of 10 µm or less. This includes particles less than 2.5 µm. Because any PM_{10} particle will generate a pulse that meets the P1 threshold, the P1 results indicate the PM_{10} particle count.

On the other hand, the $PM_{2.5}$ definition includes only particles with a diameter of 2.5 µm or less. Because only particles above 2.5 µm will generate a pulse that meets the P2 threshold, the P2 results exclude the $PM_{2.5}$ particle count.

All particles used to test this TI Design were less than 10 µm. Therefore, the test results graphs shown in Section 6 indicate the PM_{10} minus $PM_{2.5}$ particle count ($PM_{10} – PM_{2.5}$). However, in practice any particle greater than 10 µm can also be counted in the P2 result. In theory, it is possible to establish a third threshold, P3, such that particles greater than 10 µm can be subtracted from the P2 result.

5 Getting Started

5.1 Hardware Setup

Figure 13 shows the $PM_{2.5}$/PM_{10} Particle Sensor AFE Design hardware.

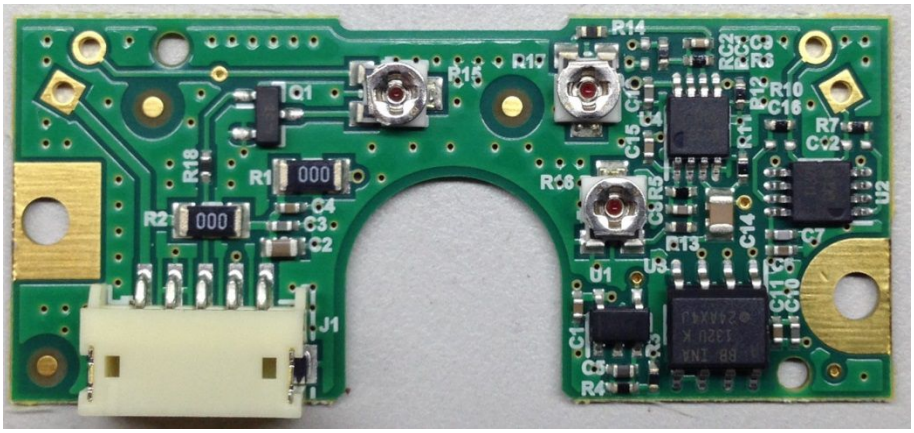

Figure 13. Particle Sensor Hardware

Three potentiometers are used in this TI Design. Potentiometer R15 controls the amount of current that flows through the LED. Potentiometers R16 and R17 set the gain on the two amplification stages in the AFE.

Connector J1 provides an easy access to the input and output signals of the $PM_{2.5}$/PM_{10} Particle Sensor AFE Design. The pinout for connector J1 is shown in Table 6. The TI Design uses the connector header part number S5B-ZR-SM4A-TF from JST. This connector can be mated with housing part number ZHR-5, also from JST.

Table 6. Connector J1 Pinout

PIN	FUNCTION	DESCRIPTION
1	LED_VCC	LED voltage input pin (shorted to VCC_3V3 by default)
2	GND	Ground pin
3	IR_LED_CTRL	Control pin for turning LED on and off
4	VOUT	Voltage output of the AFE design
5	VCC_3V3	3.3-V input pin

5.2 Sensor Assembly

The $PM_{2.5}/PM_{10}$ Particle Sensor AFE Design is designed to attach directly to the optical chamber of the Sharp Microelectronics optical dust sensor (part number: GP2Y1010AU0F).

The LED is connected to the two through-hole pads on the top-left corner. The photodiode is connected on the top-right corner.

The metal shield from the optical dust sensor is placed on top AFE to protect against external noise sources. The two mounting holes on the printed circuit board are used to secure the metal shield and PCB to the optical chamber.

NOTE: Set the gain stages and LED current before installing the metal shield.

The fully assembled unit is shown in see Figure 14 and Figure 15.

Install the sensor assembly such that the air flow in the system carries the particle through the sensor opening. Direct air flow through the sensor opening leads to more accurate measurements. Ensure that both opening on the sensor are uncovered such that particles can flow through the sensor.

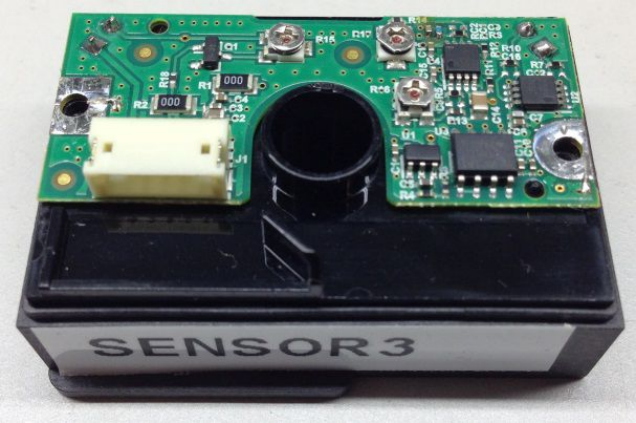

Figure 14. PCB With Optical Chamber

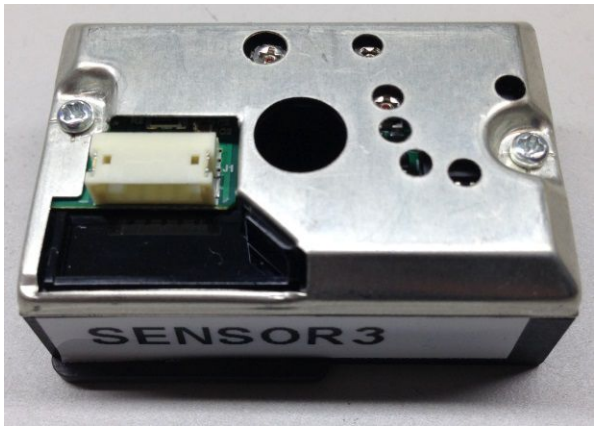

Figure 15. Fully Assembled Particle Sensor

5.3 LaunchPad™ Setup

The firmware for the $PM_{2.5}/PM_{10}$ Particle Sensor AFE Design must be loaded and run on a microprocessor. An MSP-EXP430G2 LaunchPad was used during the development of this TI Design. However, the firmware can be easily adapted to any other processor board.

Follow the steps in the TI Design firmware installer to save, load, and build the TI Design firmware. The firmware is set to the "pollen" linear calibration by default; however this can be changed through the use of a compiler directive in the main source file.

Follow these steps to interface the sensor assembly to the MSP-EXP430G2 LaunchPad:

1. Set J3 jumpers on the LaunchPad to "HW UART" mode (see silkscreen on PCB or LP UG).
2. Connect P1.4 (ADC) to the AFE voltage output on the TI AFE sensor.
3. Connect P1.5 to the LED driver pin on the TI AFE sensor.
4. Connect the GND pin on the LaunchPad to the GND pin on the TI AFE sensor.
5. Provide 3.3-V DC to the TI AFE sensor and a common GND reference between the LP and sensor.
6. Power LP from USB port.
7. Configure the serial terminal on the host to receive characters from LP UART: 9600 baud, 1 start bit, 1 stop bit, no flow control.

NOTE: Set the gain stages and LED current on the AFE before running the TI Design firmware.

6 Test Data

The $PM_{2.5}/PM_{10}$ Particle Sensor AFE Design was exposed to different types of particles using a controlled environment. The following sections describe the test setup and the results of every test and characterization performed on the design.

6.1 Test Setup

All test data was collected using an adapted version of the ANSI/AHAM AC-1-2013 "Association of Home Appliance Manufacturers Method for Measuring Performance of Portable Household Electric Room Air Cleaners" test standard. Although this test standard covers performance, testing for electric room air cleaners, the particle delivery, mixing, and monitoring methods were easily adapted to test the performance of this TI Design.

Particles were carefully delivered and mixed into the test chamber. The temperature and humidity inside the test chamber were kept constant. The particle concentration inside the test chamber was allowed to naturally decay to low levels when switching between different particle types to avoid sampling multiple particle sizes at the same time, although a test using both dust and pollen particles was also run. The test chamber had a size of 1,008 ft^3.

The concentration and natural decay (settling) rate varies significantly between dust, pollen, and smoke particles (see Table 7). Specifically, smoke particles have a very high concentration and a very slow natural decay rate. To expose the sensor to varying concentrations of particles within a reasonable amount of time, an electric air room cleaner was used during all tests to speed up the decay rate of the test particles.

Table 7. Particle Sizes and Concentration

PARTICLE TYPE	SIZE (µm)	CONCENTRATION RANGES (particles/cc)	CONCENTRATION (particles/ft^3)
Pollen	5 to 11	5 to 40	~141,600 to 1,133,000
Dust	0.5 to 3	10 to 255	~283 × 10^3 to 7.233 × 10^6
Smoke	0.10 to 1.0	12,000 to 24,000	~340 × 10^6 to 680 × 10^6

The concentration and size distribution of the test particles were monitored each second during every pollen and dust test run and every 35 seconds during every smoke test run. The sensor was placed in the direct air flow of the particle spectrometers used during the test to minimize variations in aerosol concentrations inside the test chamber.

The accuracy of the $PM_{2.5}/PM_{10}$ Particle Sensor AFE Design was calculated using two high-resolution, real-time aerodynamic particle spectrometers as references. The TSI 3321 Aerodynamic Particle Sizer Spectrometer was used for pollen and dust measurements, and the HSLAS II Airborne Particle Spectrometer was used for smoke tests. Table 8 gives a full list of the equipment that was used to test the $PM_{2.5}/PM_{10}$ Particle Sensor AFE Design. Figure 16 and Figure 17 show the location of the test equipment and sensors inside the test chamber.

Table 8. Test Equipment List

EQUIPMENT USED	MODEL NUMBER	PURPOSE
Airborne particle spectrometer	HSLAS II	Smoke particle sizing and counting
Aerodynamic particle sizer spectrometer	TSI 3321	Pollen and dust particle sizing and counting
Fluidized bed aerosol generator	TSI 3400	Dust particle generation
Temperature or humidity sensor	HMW30YB	Temperature and humidity measurement
Electric room air cleaner	Honeywell HPA100	Speed up the removal of airborne particles

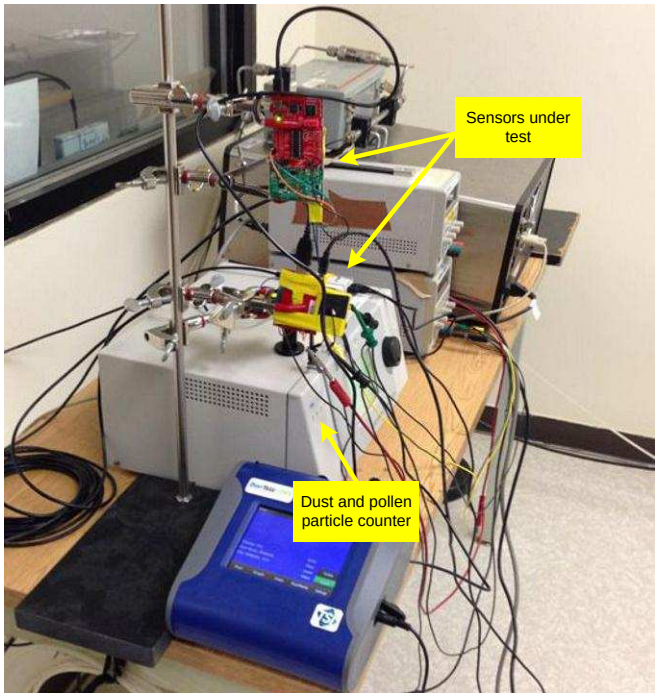

Figure 16. Pollen and Dust Test Setup

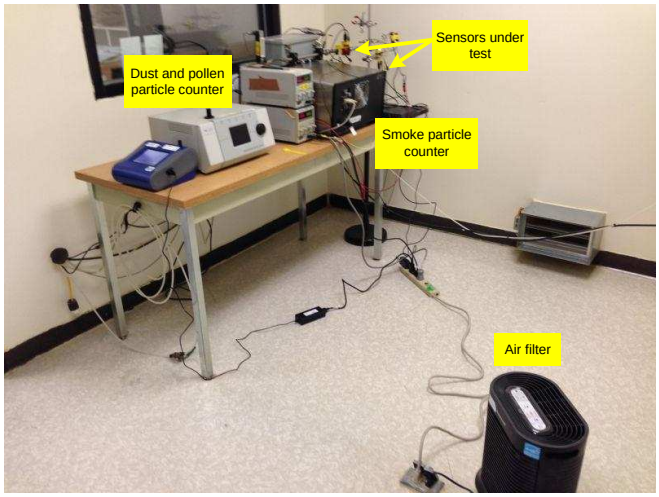

Figure 17. Smoke Test Setup

6.2 Sensor Setup

Multiple sensors were assembled as described in Section 5.2 and exposed to different concentrations of pollen, dust, and smoke particles. Power was supplied through external DC benchtop supplies.

An MSP-EXP430G2 LaunchPad implemented and ran the software algorithm as described in Section 4.5.2. The MSP430G2553 microprocessor was run at 8 MHz to provide some overhead to the computations, although given the simple architecture of the algorithm, it may have been possible to run the microprocessor at a lower frequency. The V_{OUT} signal of the sensor was sampled by the MSP430G2553 ADC with a 1-ms sampling rate and internal 1.5-V reference voltage.

All sensor data was transmitted to a host computer for post-processing using the on-chip UART. The UART was connected to a serial-to-USB adaptor to bypass the 9600 baud rate limitation of the USB serial port implemented on the MSP-EXP430G2 LaunchPad. A higher throughput connection was required in cases where raw data needed to be extracted from the sensor. For the final software implementation, data is transmitted every second and the 9600 baud rate is adequate for this purpose.

For all final tests, the LED current was set to 40 mA and the gain was set to maximum on the two amplifier stages.

6.3 Noise Testing

The noise mean, variance, and standard deviation were measured for two particle sensors. In these tests, the sensor opening was covered such that no particles could enter the sensor. The V_{OUT} of the AFE was logged for more than 15 minutes using the MSP430 ADC with a 1-ms sampling rate, an eight-sample moving average, and an internal 1.5-V reference voltage.

With no stimulus, the output of the sensors remained below an ADC count of 20, which is equivalent to ~29 mV given the 1.5-V voltage reference of the ADC. The histogram of the ADC codes for each sensor is shown in Figure 18 and Figure 19. Each figure also contains the noise mean, variance, and standard deviation results.

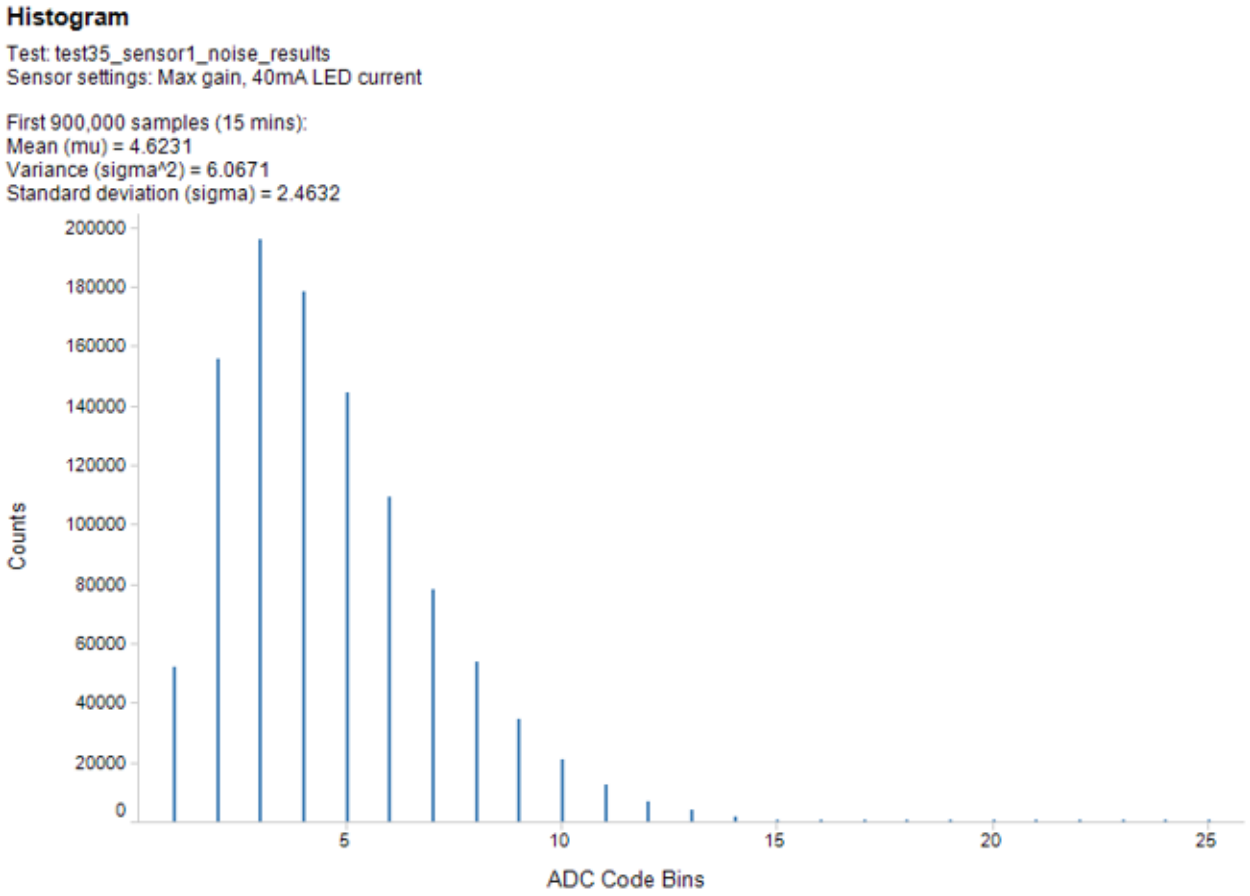

Figure 18. Histogram of ADC Codes During Noise Test For Sensor 1

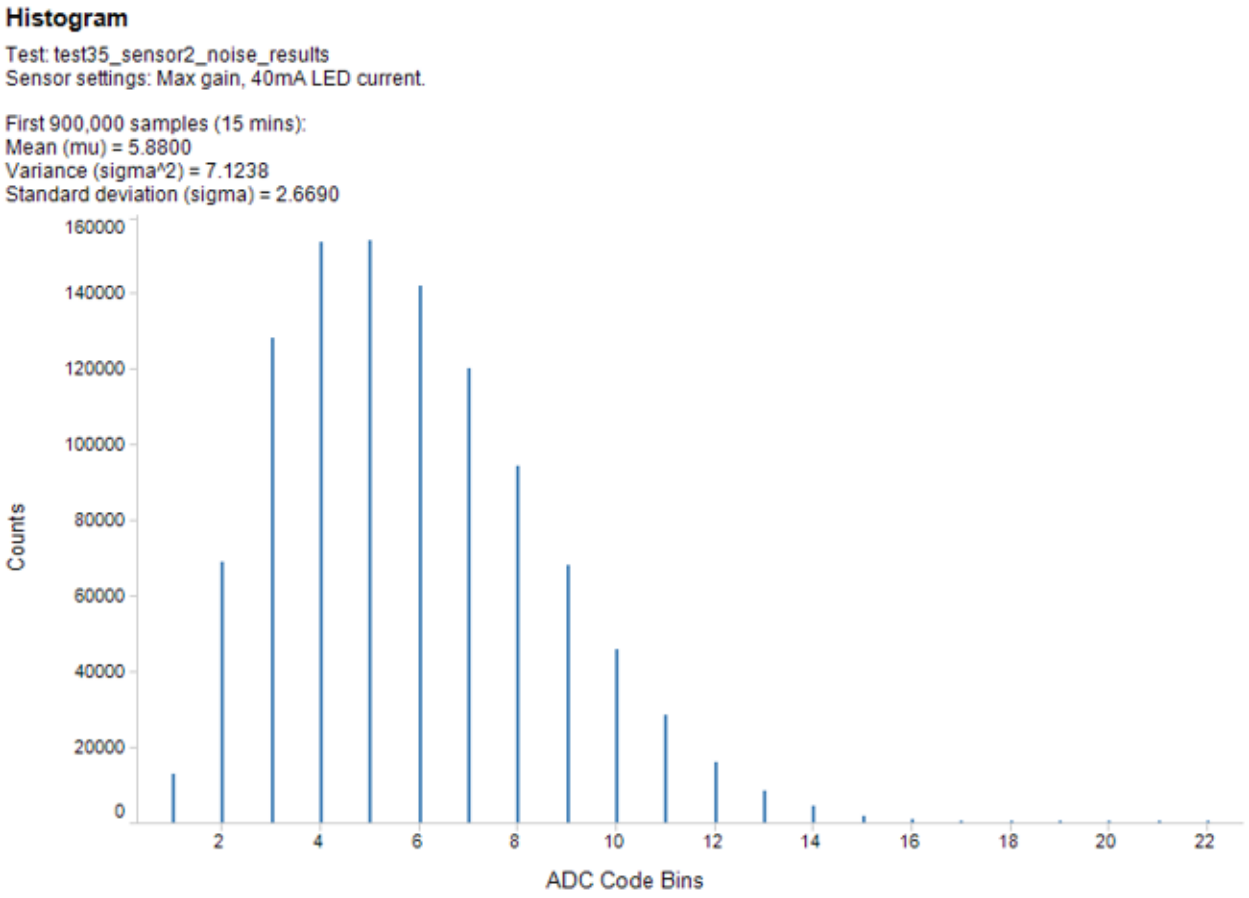

Figure 19. Histogram of ADC Codes During Noise Test For Sensor 2

6.4 Pollen Testing

The sensor was tested using pollen particles ranging in size from 5 to 11 µm. The LED current was set to 40 mA, and R16 and R17 were set to their lowest possible resistance to maximize the gain on the two amplification stages. During the test, reference measurements were taken using the TSI 3321 Aerodynamic Particle Sizer Spectrometer. The software algorithm described in Section 4.5.2 was used to derive a particle count measurement from the output of the sensor.

As described in Section 4.5.2, every second the algorithm counts the number of pulses meeting the P1 and P2 thresholds. Figure 20 shows the pulse count for each of the two thresholds. The result of the 30-second moving average is also shown. Figure 21 plots the P1 and P2 pulse counts (with a 30-second moving average) against the actual PM_{10} and $PM_{10} - PM_{2.5}$ particle count measured by the TSI 3321. As expected, both pulse counts are highest when the particles are first injected into the test chamber and they decrease as the particle concentration decays.

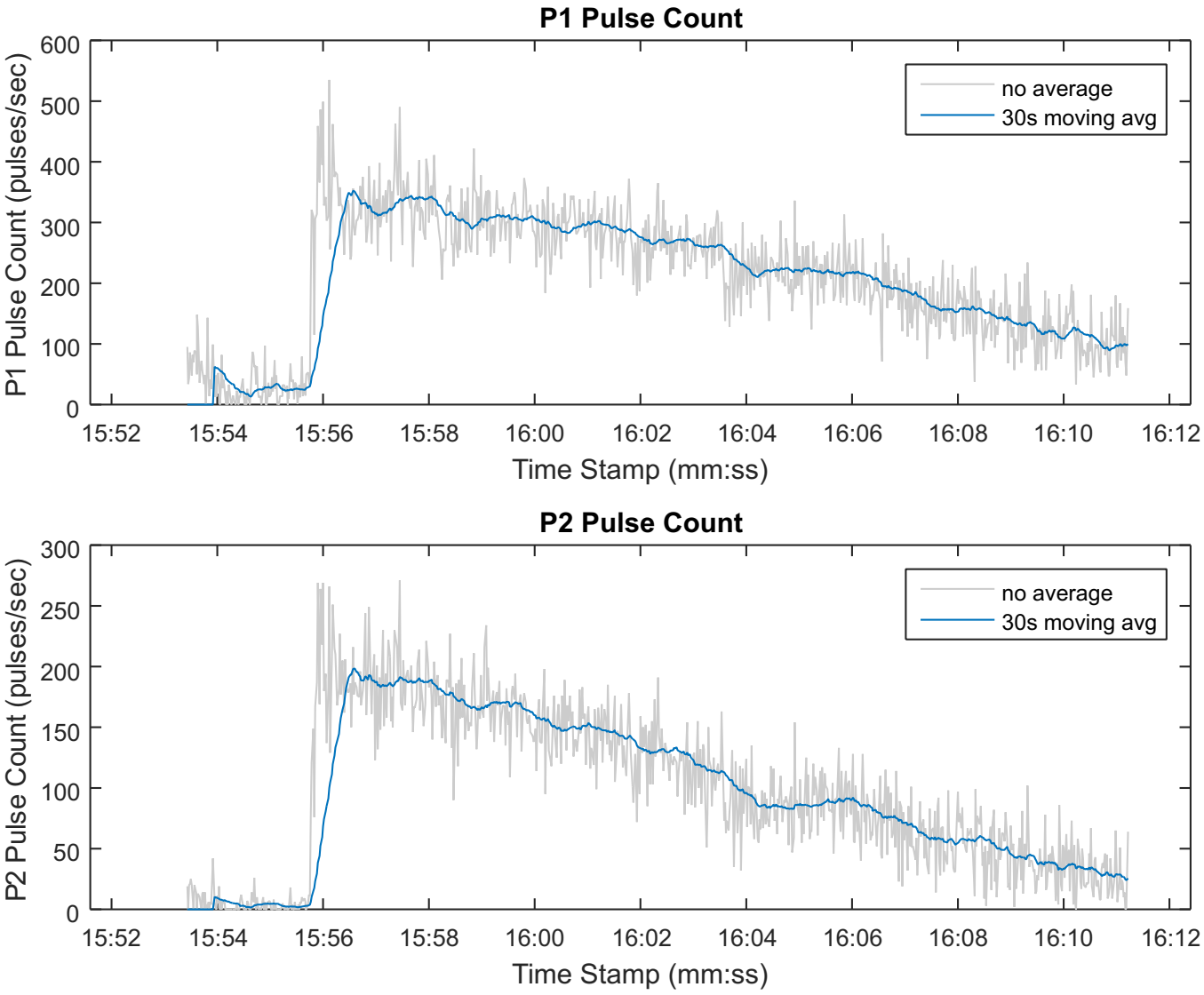

Figure 20. P1 and P2 Pulse Counts for Pollen Test

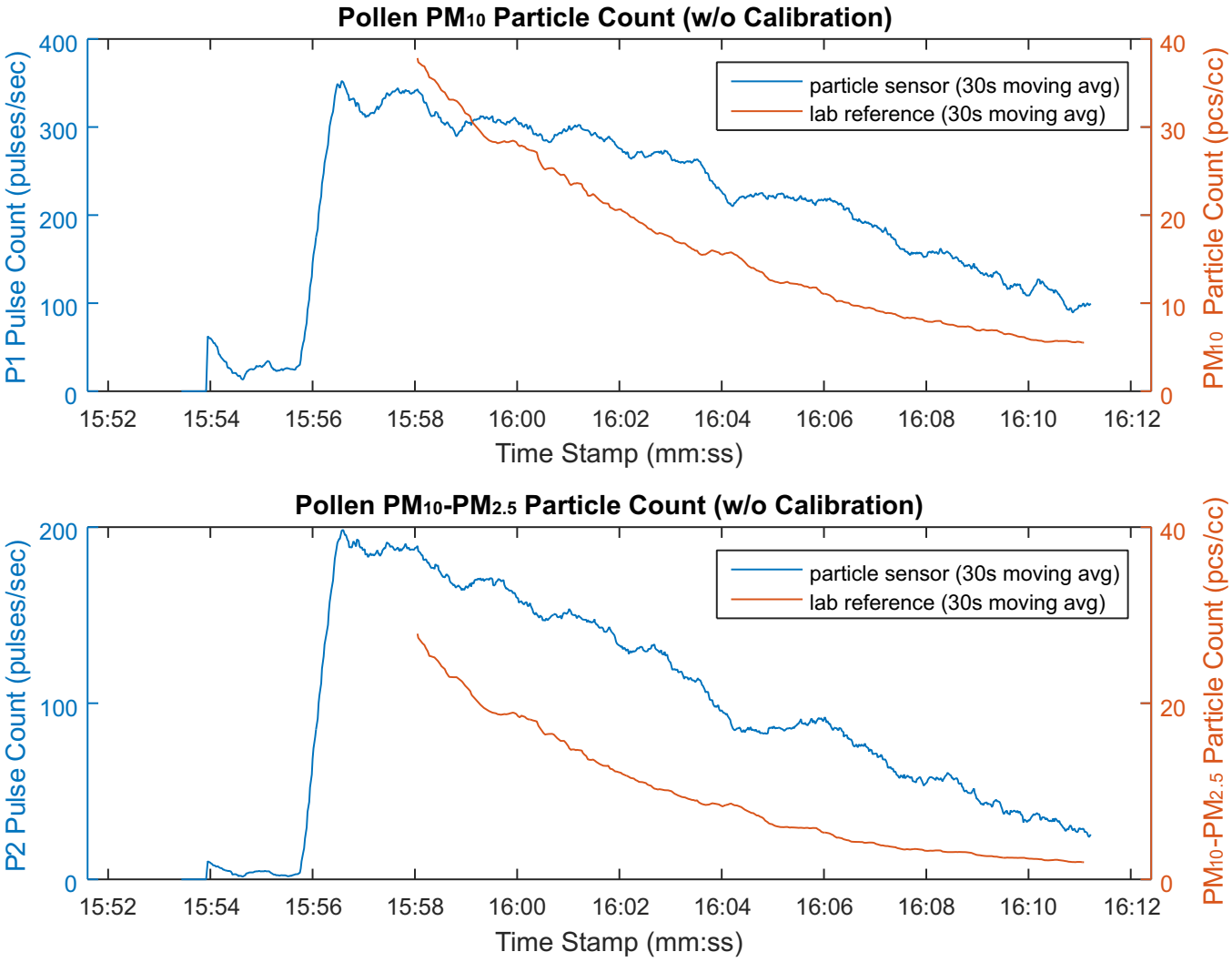

Figure 21. P1 and P2 Pulse Count versus Actual Particle Count for Pollen Test

The algorithm applies a linear calibration factor to the P1 and P2 pulse count data to calculate the final particle count measurement. The linear calibration parameters were derived through analyzing the pollen test data. The output of the particle sensing algorithm after calibration is shown in Figure 22 and Figure 23.

The output of the particle sensing algorithm is compared against the reading provided by the TSI 3321 using a standard percent error calculation. The result of the percent error calculation is shown in Figure 24 and Figure 25. As shown in the figures, the percent error increases as the particle concentration decreases. For a further discussion on these and other results, see Section 6.8.

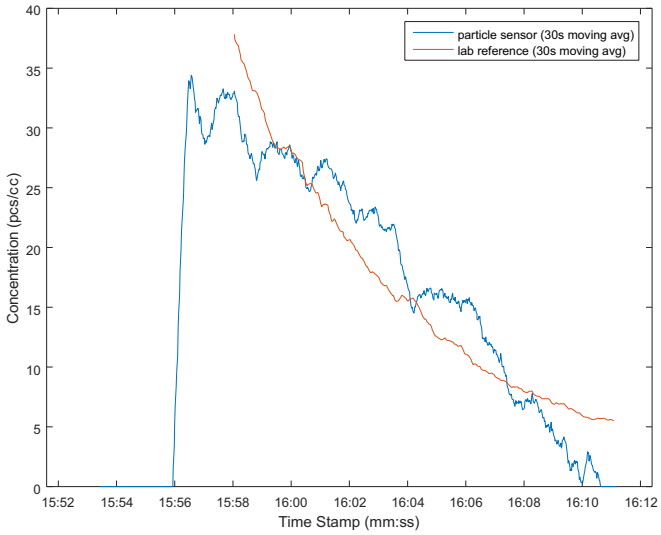

Figure 22. PM_{10} Sensor Reading After Calibration for Pollen Test

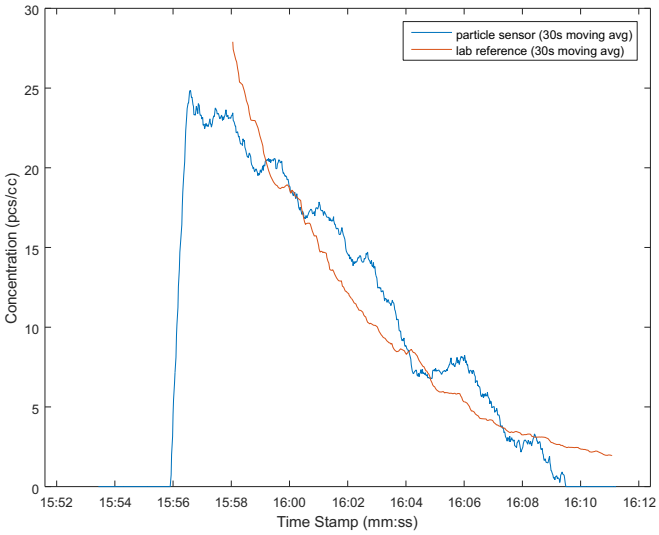

Figure 23. PM_{10} – $PM_{2.5}$ Sensor Reading After Calibration for Pollen Test

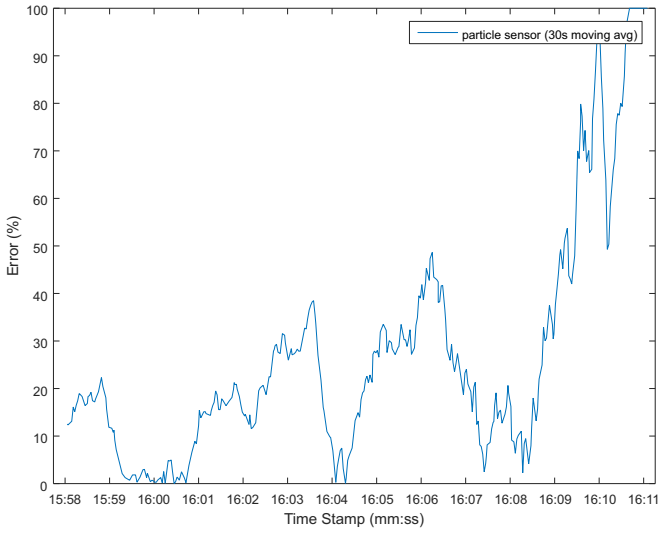

Figure 24. PM_{10} Pollen Particle Concentration Measurement Error

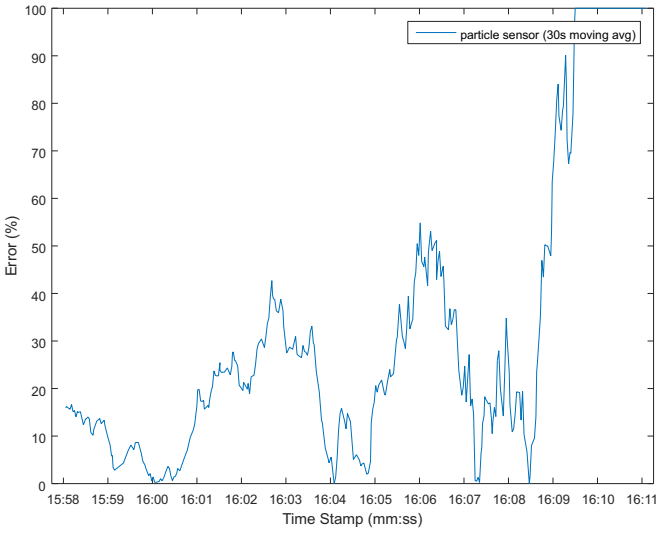

Figure 25. PM_{10} – $PM_{2.5}$ Pollen Particle Concentration Measurement Error

6.5 Dust Testing

The sensor was tested using dust particles ranging in size from 0.5 to 3 µm. The sensor was configured with an LED current of 40 mA and maximum gain on the two amplification stages. During the test, reference measurements were taken using the TSI 3321 Aerodynamic Particle Sizer Spectrometer. The software algorithm described in Section 4.5.2 was used to derive a particle count measurement from the output of the sensor.

As described in Section 4.5.2, every second the algorithm counts the number of pulses meeting the P1 and P2 thresholds. Figure 26 shows the pulse count for each of the two thresholds. The result of the 30-second moving average is also shown. Figure 27 plots the result of the P1 and P2 pulse counts (with a 30-second moving average) against the actual PM_{10} and $PM_{10} – PM_{2.5}$ particle count measured by the TSI 3321. As expected, both pulse counts are highest when the particles are first injected into the test chamber and they decrease as the particle concentration decays.

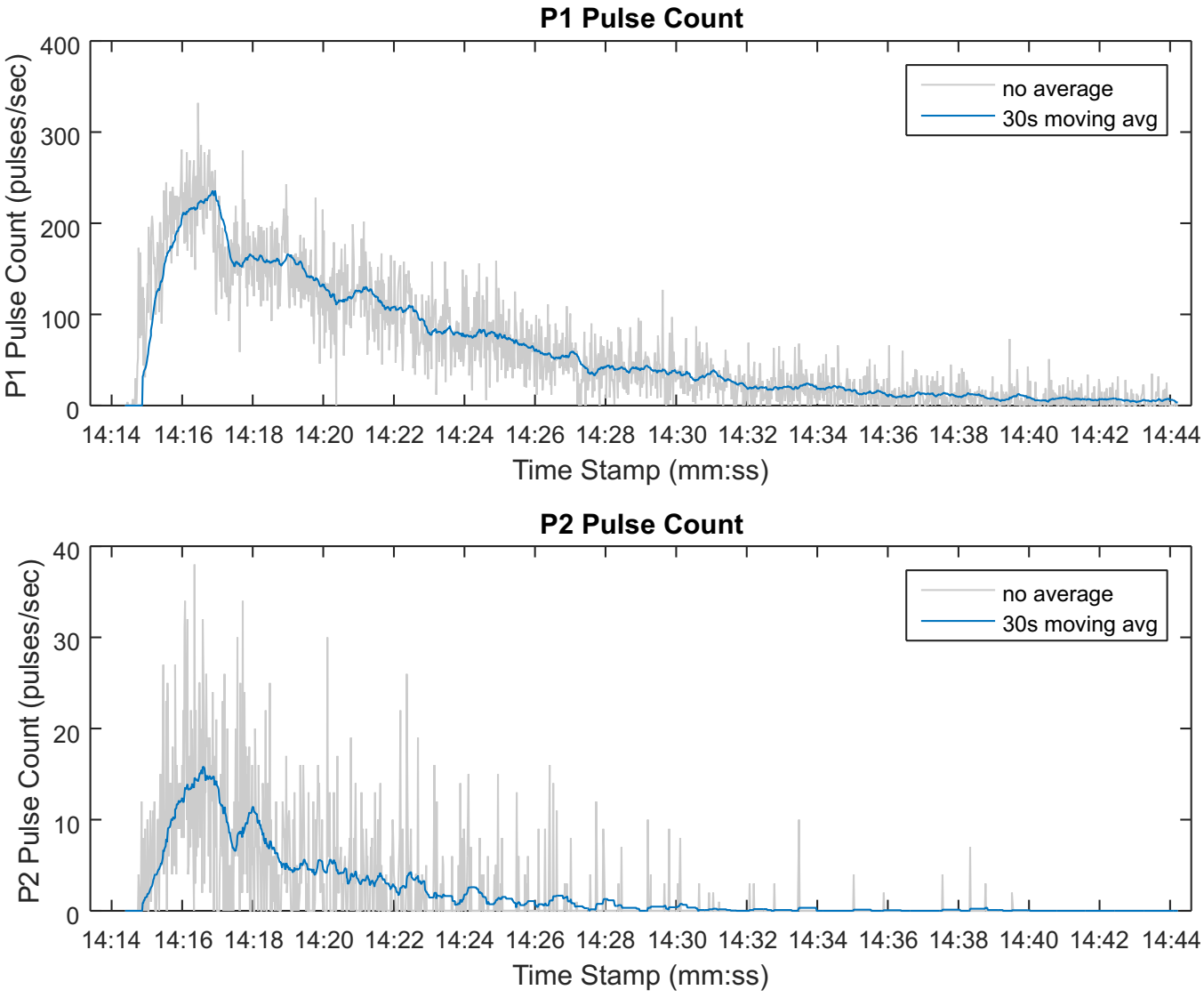

Figure 26. P1 and P2 Pulse Counts for Dust Test

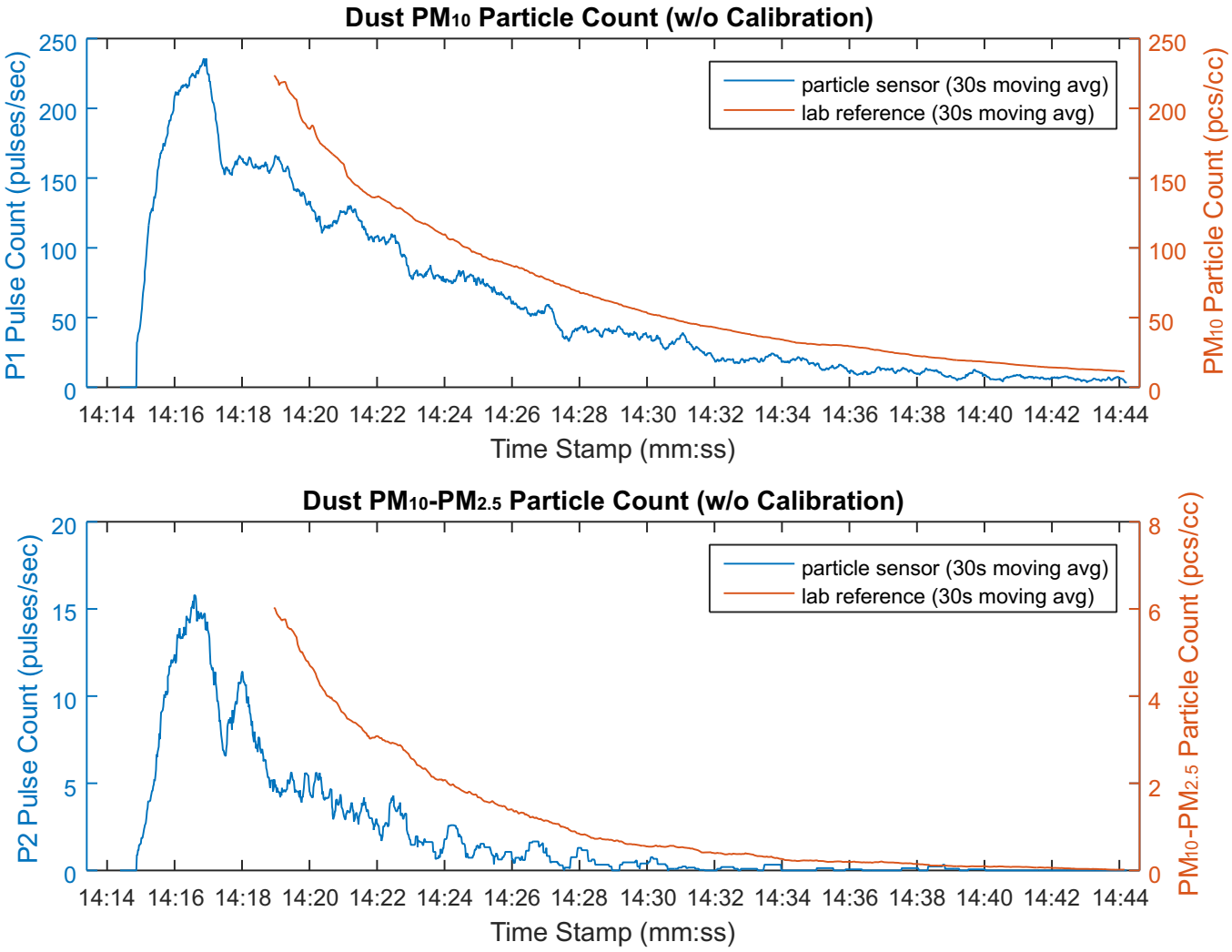

Figure 27. P1 and P2 Pulse Count versus Actual Particle Count for Dust Test

The algorithm applies a linear calibration factor to the P1 and P2 pulse count data to calculate the final particle count measurement. The linear calibration parameters were derived through analysis of the dust test data. The output of the particle sensing algorithm after calibration is shown in Figure 28 and Figure 29.

The output of the particle sensing algorithm is compared against the reading provided by the TSI 3321 Aerodynamic Particle Sizer Spectrometer using a standard percent error calculation. The result of the percent error calculation is shown in Figure 30 and Figure 31. As shown in the figures, the PM_{10} percent error increases as the particle concentration decreases. The PM_{10} – $PM_{2.5}$ percent error goes off the chart due to the very small readings provided by the TSI 3321 towards the end of the test.

One possible explanation for the high error rate in the PM_{10} – $PM_{2.5}$ measurement is the low concentration of particles with a diameter between 2.5 and 10 µm is compared to the concentration of particles with a diameter less than 2.5 µm. This low concentration causes the pulse count of the sensor to fluctuate from reading to reading leading to the higher error rate. For a further discussion on these and other results see Section 6.8.

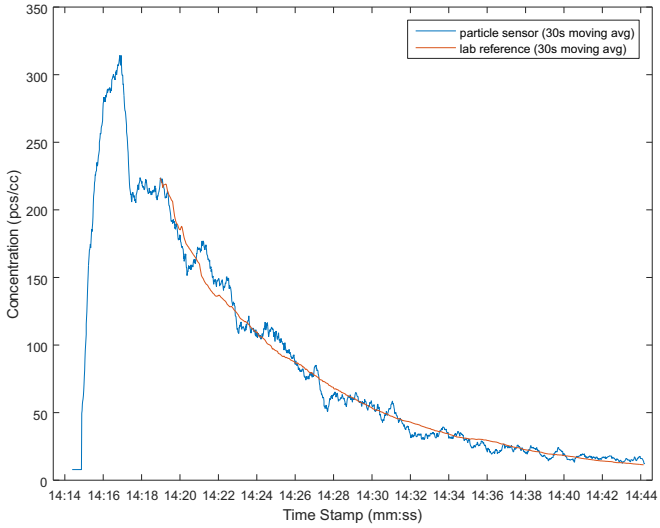

Figure 28. PM_{10} Sensor Reading After Calibration for Dust Test

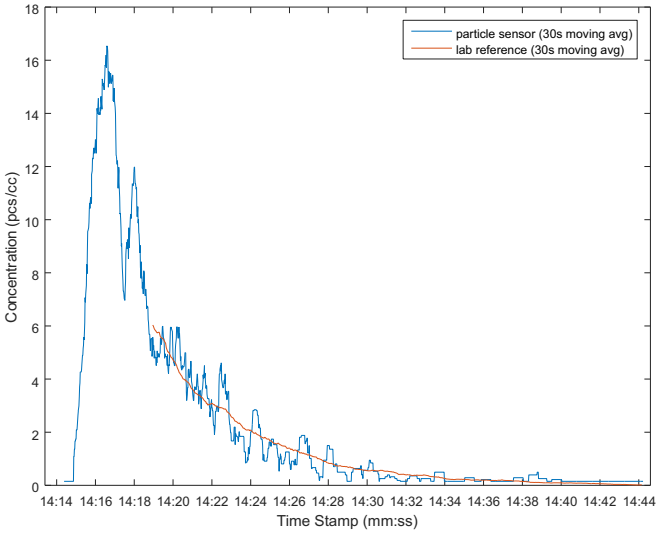

Figure 29. PM_{10} – $PM_{2.5}$ Sensor Reading After Calibration for Dust Test

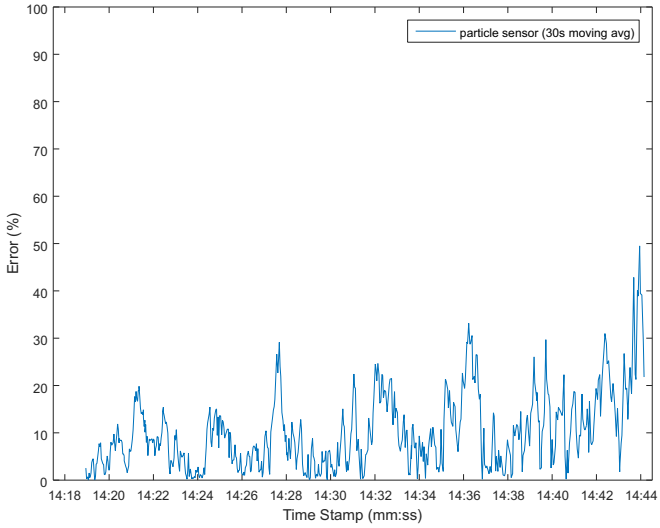

Figure 30. PM_{10} Dust Particle Concentration Measurement Error

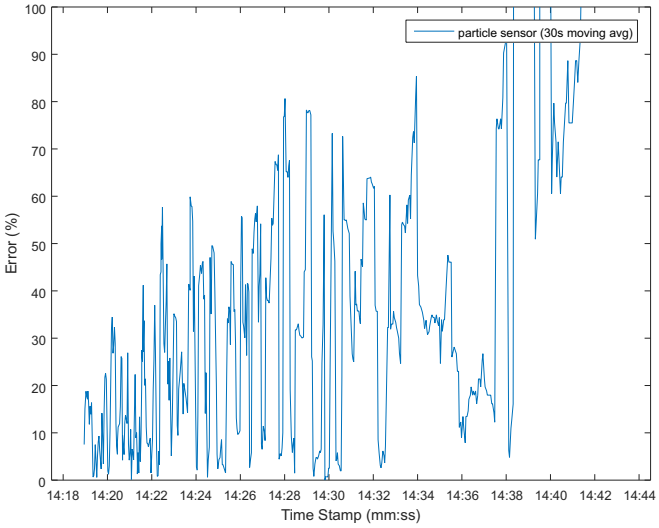

Figure 31. PM_{10} – $PM_{2.5}$ Dust Particle Concentration Measurement Error

NOTE: On Figure 31, the y-axis limited to 100%.

6.6 Smoke Testing

The sensor was tested using smoke particles ranging in size from 0.10 to 1.0 µm. The LED current was set to 40 mA and R16 and R17 were set to their lowest possible resistance to maximize the gain on the two amplification stages. During the test, reference measurements were taken using the HSLAS II Airborne Particle Spectrometer. The software algorithm described in Section 4.5.2 was used to derive a particle count measurement from the output of the sensor.

As described in Section 4.5.2, every second the algorithm counts the number of pulses meeting the P1 and P2 thresholds. Figure 32 shows the pulse count for each of the two thresholds. The result of the P1 and P2 pulse counts (with a 10-second moving average) is also shown. Figure 33 plots the result of the 10-second moving average against the actual $PM_{2.5}$ particle count measured by the HSLAS II.

Note that, unlike smoke and pollen, only PM_{10} measurement and error rate graphs are shown. This is due to the fact that there are essentially no smoke particles with a diameter above 2.5 µm and, therefore, the P2 count result of the particle sensing algorithm is essentially zero.

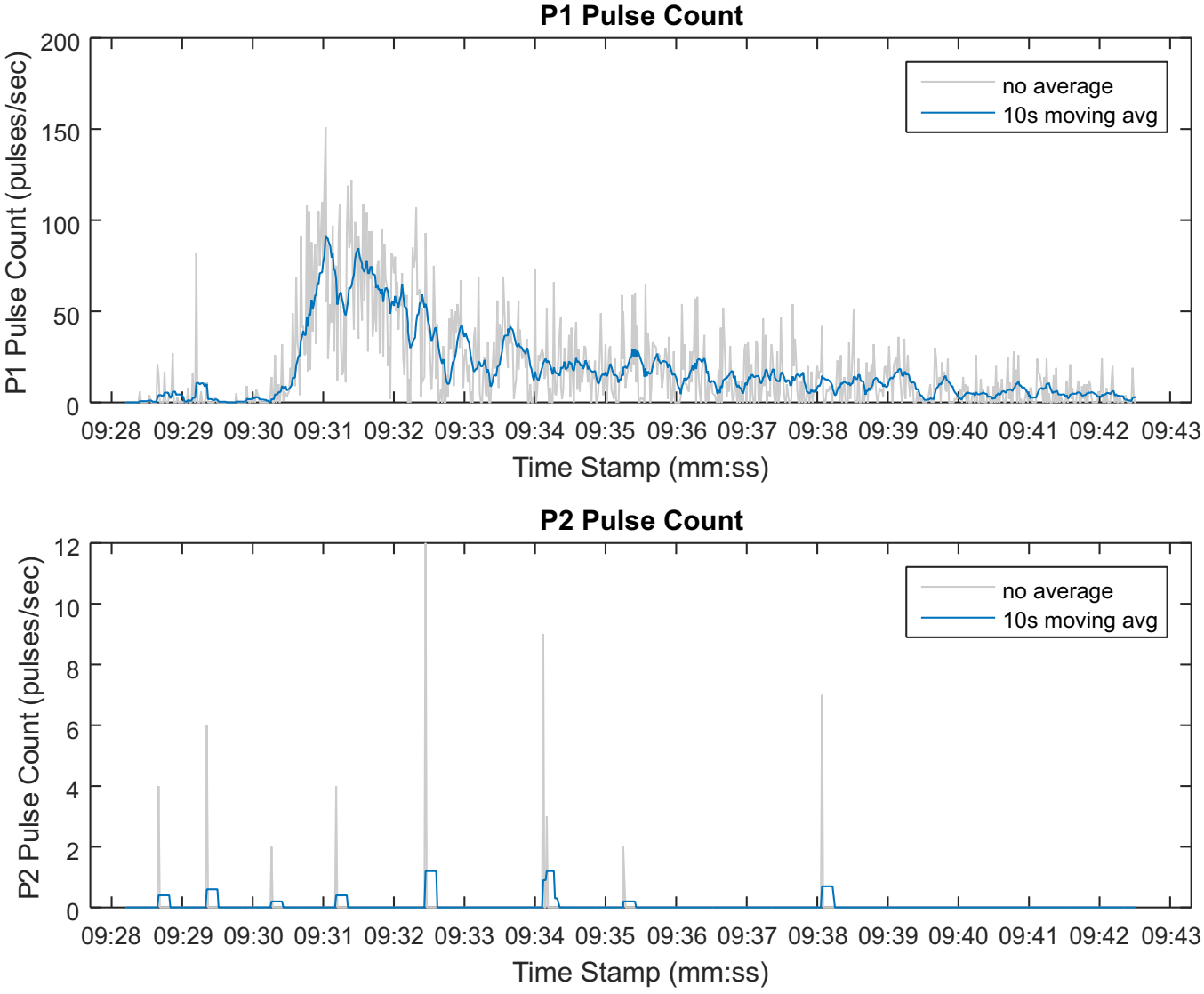

Figure 32. P1 and P2 Pulse Counts for Smoke Test

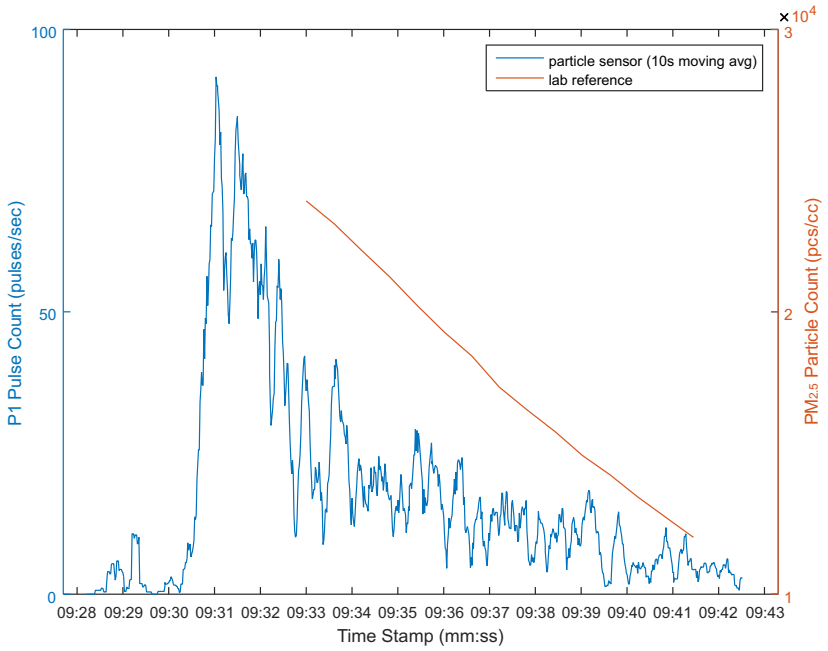

Figure 33. P1 Count versus Actual Particle Count for Smoke Test

The algorithm applies a linear calibration factor to the P1 and P2 pulse count data to calculate the final particle count measurement. The linear calibration parameters were derived through analysis of the smoke test data. The output of the particle sensing algorithm after calibration is shown in Figure 34.

The output of the particle sensing algorithm is compared against the reading provided by the HSLAS II Airborne Particle Spectrometer using a standard percent error calculation. The result of the percent error calculation is shown in Figure 35. As shown in Figure 35, the PM_{10} percent error is less than 20%. Note that the HSLAS II had a sampling rate of 35 seconds; therefore, there is less reference data for the percent error calculation.

For a further discussion on these and other results, see Section 6.8.

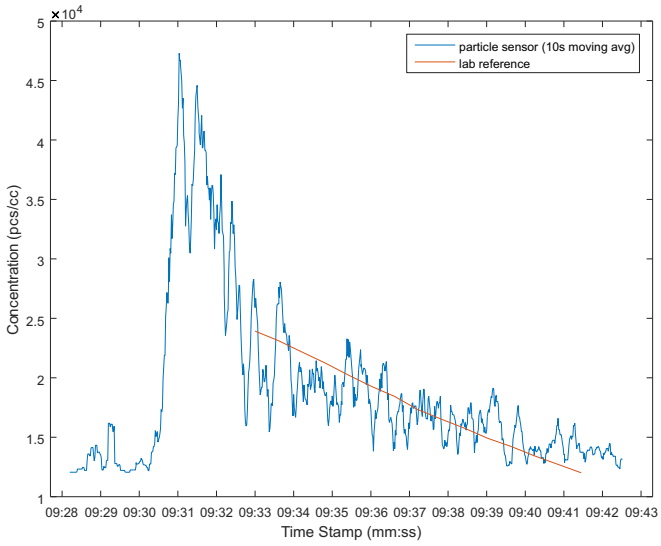

Figure 34. PM_{10} Sensor Reading After Calibration for Smoke Test

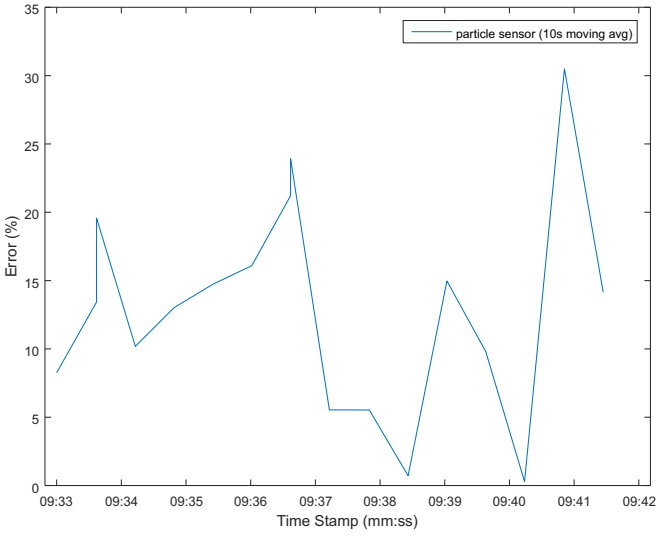

Figure 35. PM_{10} Smoke Particle Concentration Measurement Error

6.7 Combined Particle Testing

A test was carried out where a small number of dust particles were injected in the test chamber alongside pollen particles. The LED current was set to 40 mA and R16 and R17 were set to their lowest possible resistance to maximize the gain on the two amplification stages. During the test, reference measurements were taken using the TSI 3321 Aerodynamic Particle Sizer Spectrometer. The software algorithm described in Section 4.5.2 was used to derive a particle count measurement from the output of the sensor. The calibration parameters derived for pollen were used in this test. The output of the particle sensing algorithm after calibration is shown in Figure 36 and Figure 37.

The output of the particle sensing algorithm is compared against the reading provided by the TSI 3321 Aerodynamic Particle Sizer Spectrometer using a standard percent error calculation. The result of the percent error calculation is shown in Figure 38 and Figure 39. As shown in these figures, the percent error increases as the particle concentration decreases. The reason for the higher error rate in the PM_{10}–$PM_{2.5}$ measurement is because this test used the linear calibration developed for pollen particles. This calibration is not adequate for dust particles because they have different light scattering characteristics. A better algorithm would apply a different calibration algorithm depending on the particle type. However, as discussed in Section 4.5.1, pollen particles have a wide range of particle sizes, making particle identification through pulse height and count (frequency) alone difficult.

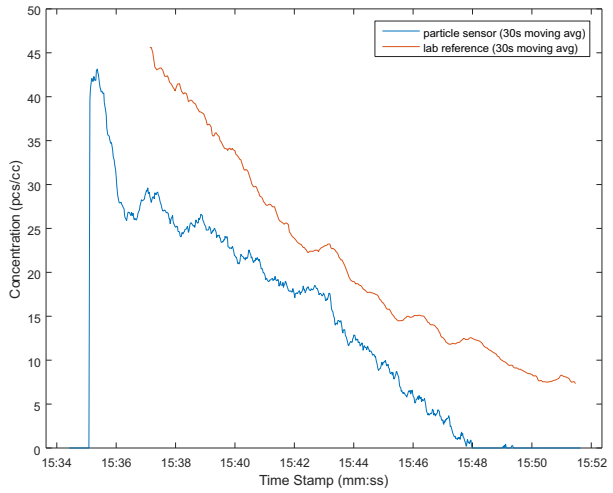

Figure 36. PM_{10} Sensor Reading Using Calibration for Pollen Particles

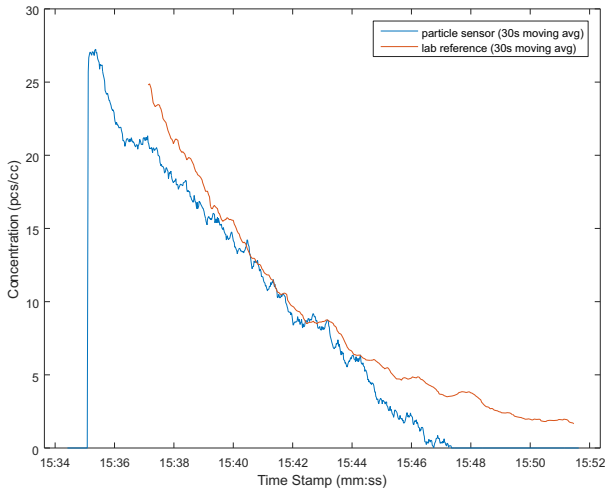

Figure 37. PM_{10} – $PM_{2.5}$ Sensor Reading Using Calibration for Pollen Particles

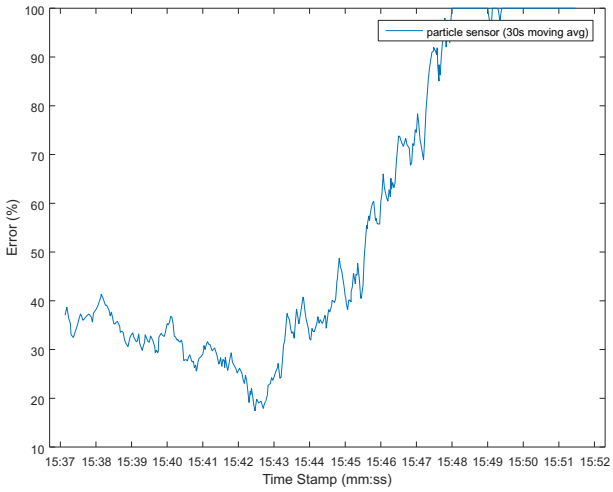

Figure 38. PM_{10} Dust and Pollen Particle Concentration Measurement Error

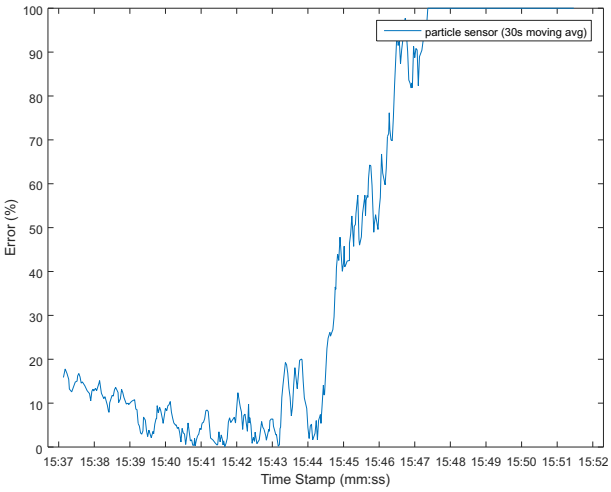

Figure 39. PM_{10} – $PM_{2.5}$ Dust and Pollen Particle Concentration Measurement Error

6.8 Discussion of Results

The results presented in this section are inline with the single LED and photodetector architecture of the $PM_{2.5}/PM_{10}$ Particle Sensor AFE for Air Quality Monitoring Design. However, the accuracy of the $PM_{2.5}/PM_{10}$ Particle Sensor AFE Design could be further improved using different methods described in this section.

First, increasing the size of the moving average effectively reduces the fluctuation in the output of the particle sensing algorithm, which can lead to more accurate results. Figure 40, Figure 42, and Figure 44 show the PM_{10} output of the particle sensing algorithm for dust particles with a 10-, 30-, and 60-second moving average in place, respectively. Figure 41, Figure 43, and Figure 45 show the result of the percent error calculation in each case. The figures show the results become more accurate as the moving average window is increased. Increasing the moving average window size can mask fast changing particle concentrations; therefore, the final window size value has to be selected according to the application requirements.

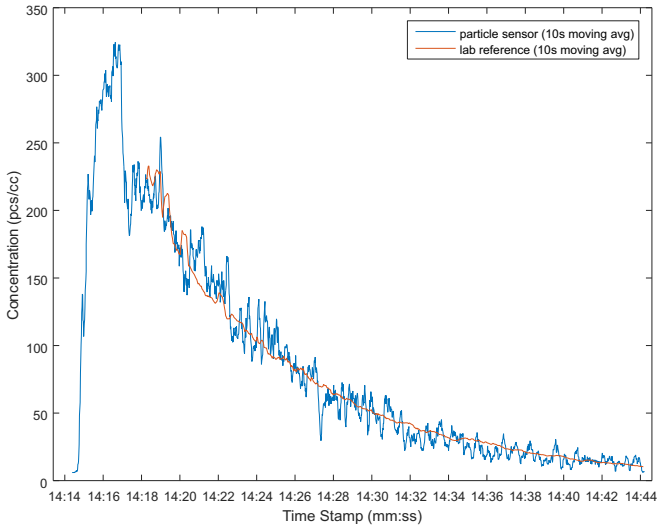

Figure 40. PM_{10} Sensor Reading After Calibration for Dust Test With 10-Second Moving Average

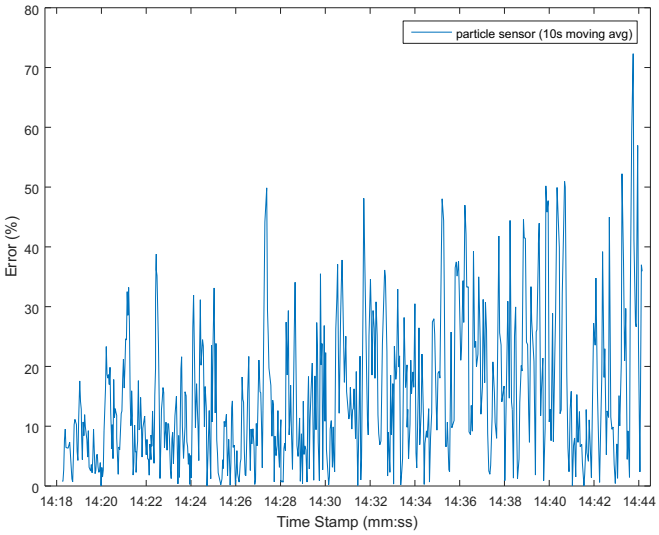

Figure 41. PM_{10} Dust Particle Concentration Measurement Error With 10-Second Moving Average

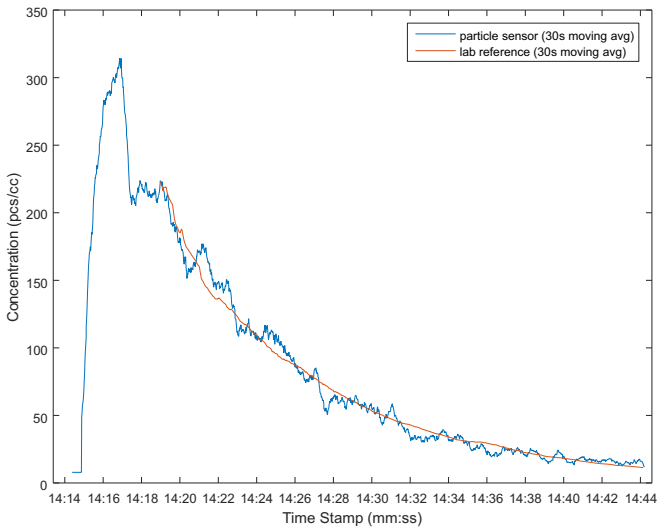

Figure 42. PM_{10} Sensor Reading After Calibration for Dust Test With 30-Second Moving Average

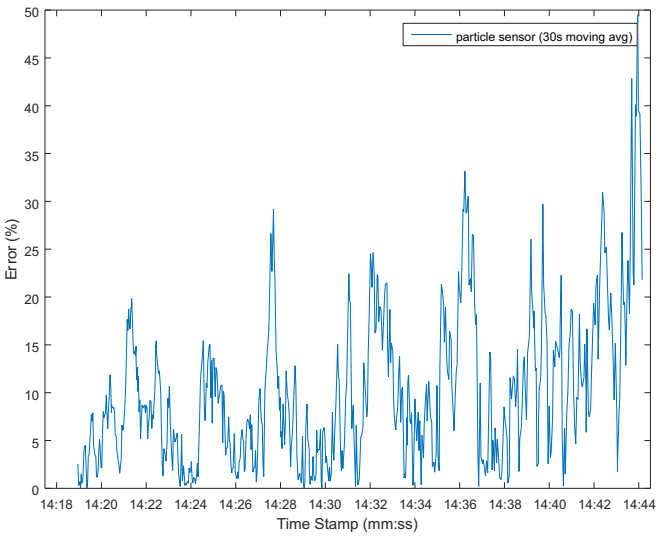

Figure 43. PM_{10} Dust Particle Concentration Measurement Error With 30-Second Moving Average

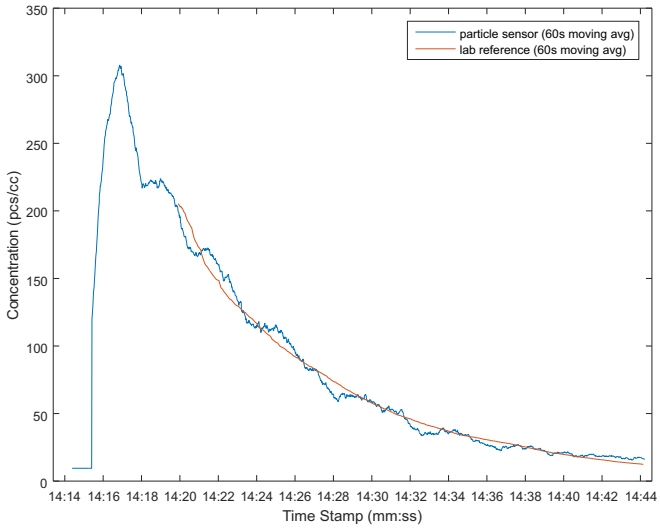

Figure 44. PM_{10} Sensor Reading After Calibration for Dust Test With 60-Second Moving Average

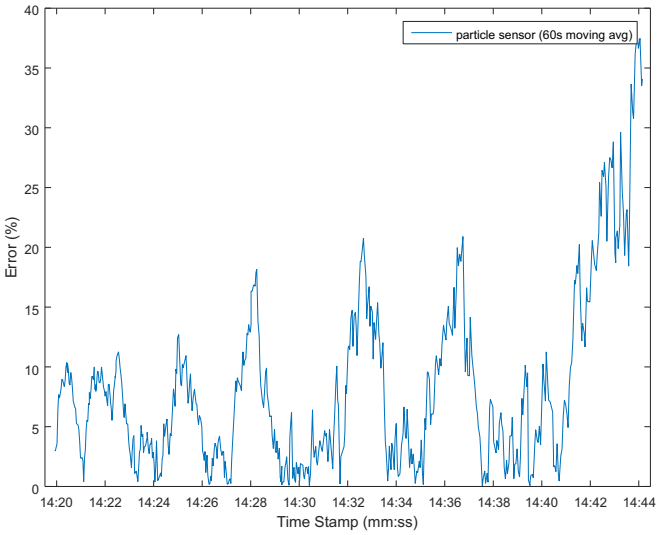

Figure 45. PM_{10} Dust Particle Concentration Measurement Error With 60-Second Moving Average

Second, focusing the calibration step on a target range of particle concentrations can lead to better results. Figure 46 and Figure 47 show the PM_{10} concentration result and percent error calculation when the input dust concentration is limited to 12 and 35 pcs/cc. The final target range of particle concentrations depends on the application requirements.

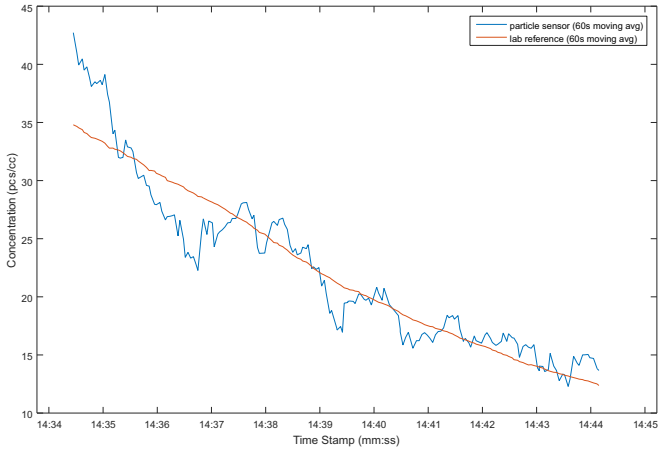

Figure 46. PM_{10} Sensor Reading After Calibration For Target Concentration Between 12 and 35 pcs/cc

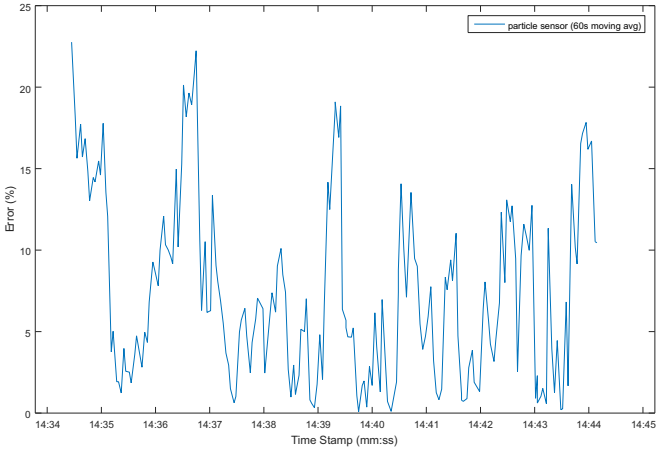

Figure 47. PM_{10} Dust Particle Concentration Measurement Error For Target Concentration Between 12 and 35 pcs/cc

Third, the use of a higher-order calibration function can lead to better results. During the algorithm development portion of this TI Design, a linear curve fit model was used to match the sensor output to the TSI 3321 and HSLAS II particle spectrometers output. Figure 48 shows that a higher-order curve fit model could lead to more accurate results.

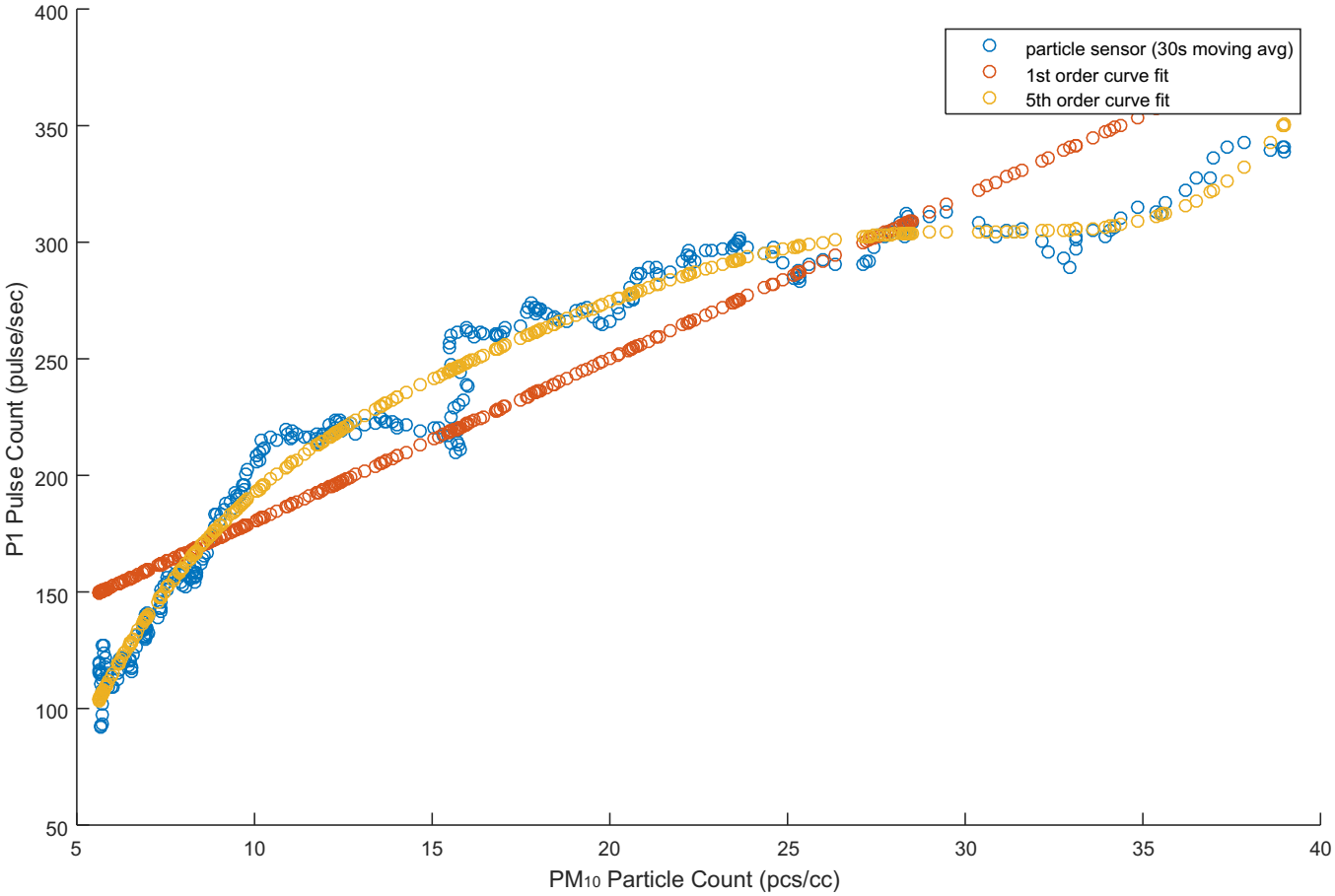

Figure 48. Pollen P1 Pulse Count Curve Fitting Using Higher Order Models

Lastly, sophisticated equipment such as the TSI 3321 Aerodynamic Particle Sizer Spectrometer and the HSLAS II Airborne Particle Spectrometer achieve highly-accurate measurements through the use of size-selective inlets, controlled air flow, laser optics, and advanced signal processing algorithms. The techniques are outside the scope of this TI Design. However, in certain applications, these techniques could be used to increase the accuracy of any particle sensor design.

6.9 Power Consumption

The power consumption of the AFE portion of the TI Design was tested with the gains on the amplification stages set to maximum. The current reading was an average of 13 mA with the TI Design running at 3.3 V. The LED driver current is not included in this measurement.

7 Design Files

7.1 Schematics

To download the schematics, see the design files at TIDA-00378.

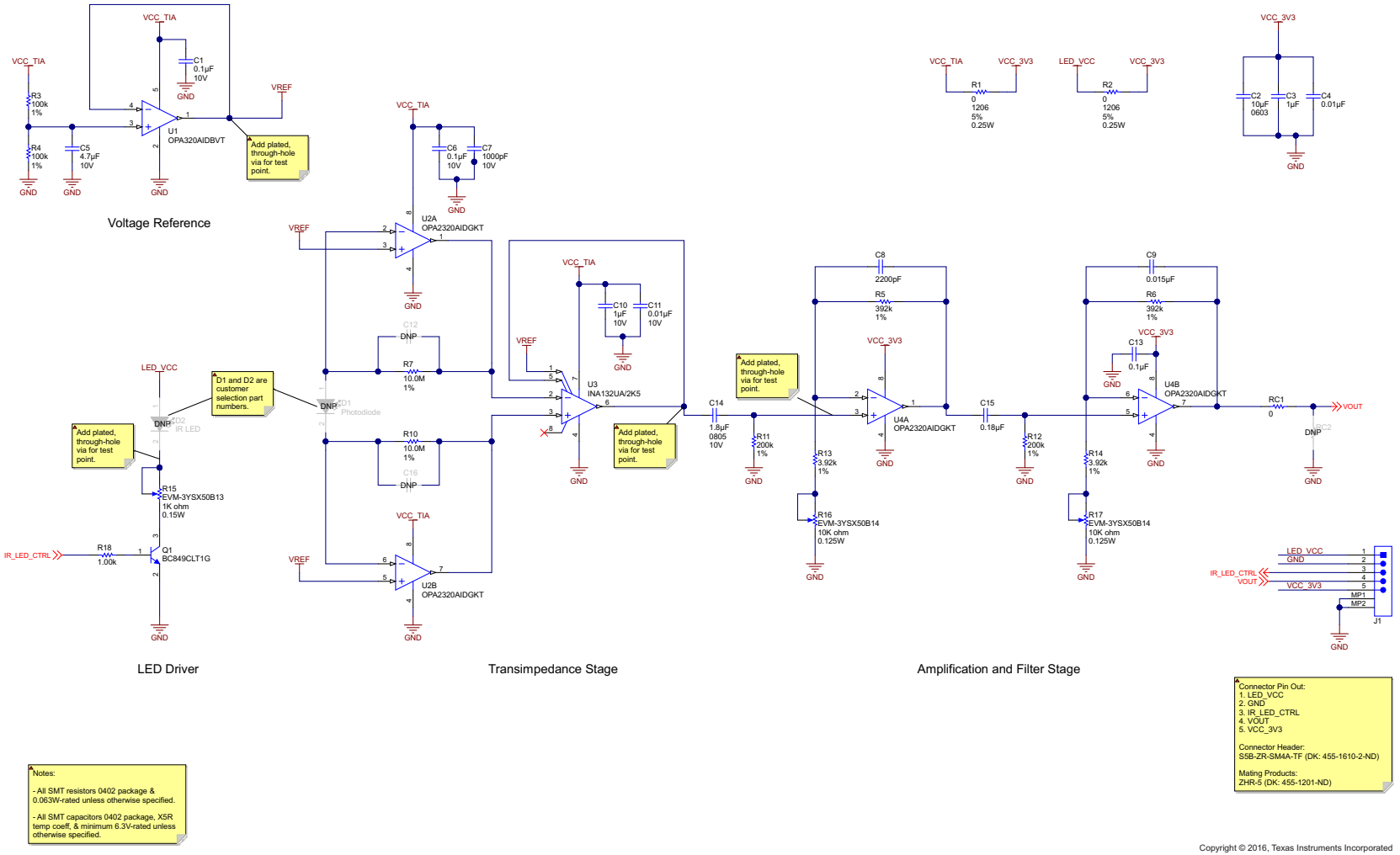

Figure 49. Particle Sensor Schematic

7.2 Bill of Materials

To download the bill of materials (BOM), see the design files at TIDA-00378.

Table 9. BOM

ITEM	DESIGNATOR	QTY	VALUE	PARTNUMBER	MANUFACTURER	DESCRIPTION	PACKAGE REFERENCE
1	!PCB1	1		ISE4043	Any	Printed Circuit Board	
2	C1, C6	2	0.1uF	C1005X5R1A104K	TDK	CAP, CERM, 0.1 µF, 10 V, +/- 10%, X5R, 0402	0402
3	C2	1	10uF	C0603C106M9PACTU	Kemet	CAP, CERM, 10 µF, 6.3 V, +/- 20%, X5R, 0603	0603
4	C3, C10	2	1uF	C1005X5R1A105K050BB	TDK	CAP, CERM, 1 µF, 10 V, +/- 10%, X5R, 0402	0402
5	C4	1	0.01uF	GRM155R60J103KA01D	MuRata	CAP, CERM, 0.01 µF, 6.3 V, +/- 10%, X5R, 0402	0402
6	C5	1	4.7uF	C1005X5R1A475K050BC	TDK	CAP, CERM, 4.7 µF, 10 V, +/- 10%, X5R, 0402	0402
7	C7	1	1000pF	GRM155R61A102KA01D	MuRata	CAP, CERM, 1000 pF, 10 V, +/- 10%, X5R, 0402	0402
8	C8	1	2200pF	GRM155R60J222KA01D	MuRata	CAP, CERM, 2200 pF, 6.3 V, +/- 10%, X5R, 0402	0402
9	C9	1	0.015uF	GRM155R71C153KA01D	MuRata	CAP, CERM, 0.015 µF, 16 V, +/- 10%, X7R, 0402	0402
10	C11	1	0.01uF	GRM155R61A103KA01D	MuRata	CAP, CERM, 0.01 µF, 10 V, +/- 10%, X5R, 0402	0402
11	C13	1	0.1uF	C1005X5R0J104K	TDK	CAP, CERM, 0.1 µF, 6.3 V, +/- 10%, X5R, 0402	0402
12	C14	1	1.8uF	C0805C185K8PACTU	Kemet	CAP, CERM, 1.8 µF, 10 V, +/- 10%, X5R, 0805	0805
13	C15	1	0.18uF	GRM155R60J184KE01D	MuRata	CAP, CERM, 0.18 µF, 6.3 V, +/- 10%, X5R, 0402	0402
14	J1	1		S5B-ZR-SM4A-TF(LF)(SN)	JST Manufacturing	Header(Shrouded), 1.5mm, 5x1, Tin, R/A, TH	Header(Shrouded), 1.5mm, 5x1, R/A, TH
15	Q1	1	30 V	BC849CLT1G	ON Semiconductor	Transistor, NPN, 30 V, 0.1 A, SOT-23	SOT-23
16	R1, R2	2	0	ERJ-8GEY0R00V	Panasonic	RES, 0, 5%, 0.25 W, 1206	1206
17	R3, R4	2	100k	RC1005F104CS	Samsung Electro-Mechanics	RES, 100 k, 1%, 0.063 W, 0402	0402
18	R5, R6	2	392k	CRCW0402392KFKED	Vishay-Dale	RES, 392 k, 1%, 0.063 W, 0402	0402
19	R7, R10	2	10.0Meg	CRCW040210M0FKED	Vishay-Dale	RES, 10.0 M, 1%, 0.063 W, 0402	0402
20	R11, R12	2	200k	CRCW0402200KFKED	Vishay-Dale	RES, 200 k, 1%, 0.063 W, 0402	0402

Table 9. BOM (continued)

ITEM	DESIGNATOR	QTY	VALUE	PARTNUMBER	MANUFACTURER	DESCRIPTION	PACKAGE REFERENCE
21	R13, R14	2	3.92k	CRCW04023K92FKED	Vishay-Dale	RES, 3.92 k, 1%, 0.063 W, 0402	0402
22	R15	1	1K ohm	EVM-3YSX50B13	Panasonic	TRIMMER, 1K Ohm, 0.15W, SMD	3.1x3.45mm
23	R16, R17	2	10K ohm	EVM-3YSX50B14	Panasonic	TRIMMER, 10K Ohm, 0.15W, SMD	3.1x3.45mm
24	R18	1	1.00k	ERJ-2RKF1001X	Panasonic	RES, 1.00 k, 1%, 0.1 W, 0402	0402
25	RC1	1	0	ERJ-2GE0R00X	Panasonic	RES, 0, 5%, 0.063 W, 0402	0402
26	U1	1		OPA320AIDBVT	Texas Instruments	Precision, 20 MHz, 0.9 pA Ib, RRIO, CMOS Operational Amplifier, 1.8 to 5.5 V, -40 to 125 degC, 5-pin SOT23 (DBV0005A), Green (RoHS & no Sb/Br)	DBV0005A
27	U2, U4	2		OPA2320AIDGKT	Texas Instruments	Precision, 20 MHz, 0.9 pA Ib, RRIO, CMOS Operational Amplifier, 1.8 to 5.5 V, -40 to 125 degC, 8-pin SOP (DGK0008A), Green (RoHS & no Sb/Br)	DGK0008A
28	U3	1		INA132UA/2K5	Texas Instruments	Low Power, Single-Supply DIFFERENCE AMPLIFIER, D0008A	D0008A
29	C12, C16	0	4.7uF	GRM155R60J475ME87D	MuRata	CAP, CERM, 4.7 µF, 6.3 V, +/- 20%, X5R, 0402	0402
30	D1	0	Photodiode	Customer Option	Customer Option	Photodiode	T-1 3/4 LED, TH
31	D2	0	IR LED	Customer Option	Customer Option	IR LED	T-1 3/4 LED, TH
32	FID1, FID2, FID3	0		N/A	N/A	Fiducial mark. There is nothing to buy or mount.	Fiducial
33	RC2	0	0	ERJ-2GE0R00X	Panasonic	RES, 0, 5%, 0.063 W, 0402	0402

7.3 Layout Plots

To download the layout plots, see the design files at TIDA-00378.

7.4 Altium Project

To download the Altium project files, see the design files at TIDA-00378.

7.5 Layout Guidelines

The $PM_{2.5}$/PM_{10} Particle Sensor AFE Design was laid out using a four-layer PCB with all components placed on the top side. All signal routing is carried out in the top and bottom layers (see Table 10 for full PCB stack-up).

Table 10. PCB Stack-up

LAYER	PURPOSE
Top	Signal
2nd Layer	Ground
3rd Layer	Power
Bottom	Signal

The PCB outline was created to match the optical chamber design on the Sharp Microelectronics optical dust sensor (part number: GP2Y1010AU0F). The PCB size is 44 × 19 mm (1732 × 748 mils).

The PCB design can be modified as needed to match any optical chamber design. However, follow these guidelines, if possible, to ensure good performance from the AFE:

- Keep the traces connecting the photodiode to the OPA2320 (U2A and U2B) in the transimpedance stage symmetric. Shield these traces from other signals to avoid coupling any unwanted signals and noise.
- Keep the traces connecting the OPA2320 (U2A and U2B) and the INA132 (U3) in the transimpedance stage symmetric. Impedance mismatch in these two signals will offset the output of the INA132. Shield these traces from other signals to avoid coupling any unwanted signals and noise.
- Shield the trace between the INA132 (U3) and C14 from other signals to avoid coupling any unwanted signals and noise.
- Keep the decoupling capacitors for the INA132 and OPA2320 part as close as possible to the supply pins.

7.6 Gerber Files

To download the Gerber files, see the design files at TIDA-00378.

7.7 Assembly Drawings

To download the assembly drawings, see the design files at TIDA-00378.

7.8 Firmware Files

To download the firmware files, see the design files at TIDA-00378.

8 References

1. Texas Instruments, *Low Power, Single-Supply Difference Amplifier*, INA132 Datasheet (SBOS059).
2. Texas Instruments, *Precision, 20MHz, 0.9pA Ib, RRIO, CMOS Operational Amplifier with Shutdown*, OAP320, OPA2320 Datasheet (SBOS513).
3. Texas Instruments, *MSP-EXP430G2 LaunchPad Evaluation Kit*, MSP-EXP430G2 User's Guide (SLAU318).
4. Texas Instruments, *Photodiode Monitoring with Op Amps*, Application Bulletin (SBOA035).
5. Bohren, C. and D. Huffman, (1983). *Absorption and Scattering of Light by Small Particles*. New York: Wiley.
6. Kulkarni, P. (2011). *Aerosol Measurement: Principles, Techniques, and Applications* (3rd ed.). Hoboken, N.J.: Wiley.
7. United States Environmental Protection Agency, *Particulate Matter (PM)*. Retrieved November 25, 2015 (http://www.epa.gov/pm/).
8. United States Environmental Protection Agency, *National Ambient Air Quality Standards for Particulate Matter; Final Rule*, January 15, 2013. Federal Register Vol. 78, No. 10 (PDF).
9. World Health Organization, *WHO Air quality guidelines for particulate matter, ozone, nitrogen dioxide and sulfur dioxide*, Global Update 2005 (PDF).
10. European Commission, *Air Quality Standards*. (n.d.). Retrieved November 25, 2015 (http://ec.europa.eu/environment/air/quality/standards.htm).

9 About the Authors

GUSTAVO MARTINEZ is a senior systems architect at Texas Instruments where he is responsible for developing reference designs for industrial applications. Gustavo has ample experience developing system reference designs for the Smart Grid and home automation segments, which include high-performance application processors, floating-point digital signal processors, and RF technology. Gustavo obtained his master of electrical engineering degree from the University of Houston and his bachelor of science degree from the University of Texas at El Paso.

DAVID STOUT is a systems designer at Texas Instruments, where he is responsible for developing reference designs in the industrial segment. David has over 18 years of experience designing Analog, Mixed-Signal, and RF ICs with more than 14 years focused on products for the industrial semiconductor market. David earned his bachelor of science in electrical engineering (BSEE) degree from Louisiana State University, Baton Rouge, Louisiana and earned a master of science in electrical engineering (MSEE) degree from the University of Texas at Dallas, Richardson, Texas.

Revision History

NOTE: Page numbers for previous revisions may differ from page numbers in the current version.

Changes from Original (December 2015) to C Revision	Page
• Changed error in VREF input representation	3

IMPORTANT NOTICE FOR TI REFERENCE DESIGNS

Texas Instruments Incorporated ('TI") reference designs are solely intended to assist designers ("Designer(s)") who are developing systems that incorporate TI products. TI has not conducted any testing other than that specifically described in the published documentation for a particular reference design.

TI's provision of reference designs and any other technical, applications or design advice, quality characterization, reliability data or other information or services does not expand or otherwise alter TI's applicable published warranties or warranty disclaimers for TI products, and no additional obligations or liabilities arise from TI providing such reference designs or other items.

TI reserves the right to make corrections, enhancements, improvements and other changes to its reference designs and other items.

Designer understands and agrees that Designer remains responsible for using its independent analysis, evaluation and judgment in designing Designer's systems and products, and has full and exclusive responsibility to assure the safety of its products and compliance of its products (and of all TI products used in or for such Designer's products) with all applicable regulations, laws and other applicable requirements. Designer represents that, with respect to its applications, it has all the necessary expertise to create and implement safeguards that (1) anticipate dangerous consequences of failures, (2) monitor failures and their consequences, and (3) lessen the likelihood of failures that might cause harm and take appropriate actions. Designer agrees that prior to using or distributing any systems that include TI products, Designer will thoroughly test such systems and the functionality of such TI products as used in such systems. Designer may not use any TI products in life-critical medical equipment unless authorized officers of the parties have executed a special contract specifically governing such use. Life-critical medical equipment is medical equipment where failure of such equipment would cause serious bodily injury or death (e.g., life support, pacemakers, defibrillators, heart pumps, neurostimulators, and implantables). Such equipment includes, without limitation, all medical devices identified by the U.S. Food and Drug Administration as Class III devices and equivalent classifications outside the U.S.

Designers are authorized to use, copy and modify any individual TI reference design only in connection with the development of end products that include the TI product(s) identified in that reference design. HOWEVER, NO OTHER LICENSE, EXPRESS OR IMPLIED, BY ESTOPPEL OR OTHERWISE TO ANY OTHER TI INTELLECTUAL PROPERTY RIGHT, AND NO LICENSE TO ANY TECHNOLOGY OR INTELLECTUAL PROPERTY RIGHT OF TI OR ANY THIRD PARTY IS GRANTED HEREIN, including but not limited to any patent right, copyright, mask work right, or other intellectual property right relating to any combination, machine, or process in which TI products or services are used. Information published by TI regarding third-party products or services does not constitute a license to use such products or services, or a warranty or endorsement thereof. Use of the reference design or other items described above may require a license from a third party under the patents or other intellectual property of the third party, or a license from TI under the patents or other intellectual property of TI.

TI REFERENCE DESIGNS AND OTHER ITEMS DESCRIBED ABOVE ARE PROVIDED "AS IS" AND WITH ALL FAULTS. TI DISCLAIMS ALL OTHER WARRANTIES OR REPRESENTATIONS, EXPRESS OR IMPLIED, REGARDING THE REFERENCE DESIGNS OR USE OF THE REFERENCE DESIGNS, INCLUDING BUT NOT LIMITED TO ACCURACY OR COMPLETENESS, TITLE, ANY EPIDEMIC FAILURE WARRANTY AND ANY IMPLIED WARRANTIES OF MERCHANTABILITY, FITNESS FOR A PARTICULAR PURPOSE, AND NON-INFRINGEMENT OF ANY THIRD PARTY INTELLECTUAL PROPERTY RIGHTS.

TI SHALL NOT BE LIABLE FOR AND SHALL NOT DEFEND OR INDEMNIFY DESIGNERS AGAINST ANY CLAIM, INCLUDING BUT NOT LIMITED TO ANY INFRINGEMENT CLAIM THAT RELATES TO OR IS BASED ON ANY COMBINATION OF PRODUCTS AS DESCRIBED IN A TI REFERENCE DESIGN OR OTHERWISE. IN NO EVENT SHALL TI BE LIABLE FOR ANY ACTUAL, DIRECT, SPECIAL, COLLATERAL, INDIRECT, PUNITIVE, INCIDENTAL, CONSEQUENTIAL OR EXEMPLARY DAMAGES IN CONNECTION WITH OR ARISING OUT OF THE REFERENCE DESIGNS OR USE OF THE REFERENCE DESIGNS, AND REGARDLESS OF WHETHER TI HAS BEEN ADVISED OF THE POSSIBILITY OF SUCH DAMAGES.

TI's standard terms of sale for semiconductor products (http://www.ti.com/sc/docs/stdterms.htm) apply to the sale of packaged integrated circuit products. Additional terms may apply to the use or sale of other types of TI products and services.

Designer will fully indemnify TI and its representatives against any damages, costs, losses, and/or liabilities arising out of Designer's non-compliance with the terms and provisions of this Notice.

Mailing Address: Texas Instruments, Post Office Box 655303, Dallas, Texas 75265